

Post-depositional modification on seasonal and 1 interannual timescales resets the deuterium excess 2 signals in summer snow layers in Greenland

Michael Town¹, H C Steen-Larsen², S Wahl^{2,3}, A.-K Faber², M Behrens^{4,5}, M Hörhold⁴, T R Jones⁵, A Sveinbjornsdottir⁶, and A M Zuhr^{6,7}

¹Affiliation not available

²Geophysical Institute and Bjerknes Centre for Climate Research, University of Bergen

³École Polytechnique Fédérale de Lausanne

⁴Alfred-Wegener-Institut Helmholtz-Zentrum für Polar-und Meeresforschung, Research Unit

⁵Institute of Arctic and Alpine Research, University of Colorado

⁶Institute of Earth Sciences

⁷Alfred-Wegener-Institut Helmholtz-Zentrum für Polar-und Meeresforschung, Research Unit Postdam

April 18, 2023

1 **Post-depositional modification on seasonal and**
2 **interannual timescales resets the deuterium excess**
3 **signals in summer snow layers in Greenland**

4 **M. S. Town¹, H. C. Steen-Larsen¹, S. Wahl^{1,2}, A.-K. Faber¹, M. Behrens³, M.**
5 **Hörhold³, T. R. Jones⁴, A. Sveinbjornsdottir⁵, A. M. Zuhr⁶**

6 ¹Geophysical Institute and Bjerknes Centre for Climate Research, University of Bergen, Bergen, Norge

7 ²École Polytechnique Fédérale de Lausanne, Lausanne, Suisse

8 ³Alfred-Wegener-Institut Helmholtz-Zentrum für Polar- und Meeresforschung, Research Unit

9 Bremerhaven, Bremerhaven, Germany

10 ⁴Institute of Arctic and Alpine Research, University of Colorado, Boulder, USA

11 ⁵Institute of Earth Sciences, Reykjavík, Ísland

12 ⁶Alfred-Wegener-Institut Helmholtz-Zentrum für Polar- und Meeresforschung, Research Unit Postdam,

13 Postdam, Germany

14 **Key Points:**

- 15 • Deuterium-excess (d) decreases up to 5 ‰ in near-surface snow during some sum-
16 mers at EastGRIP, likely due to net sublimation.
- 17 • After one-to-two years in the snowpack, the peak d shifts from Autumn snow lay-
18 ers towards Summer snow layers.
- 19 • Isotope-gradient diffusion explains some but not all of the d seasonality changes
20 in the near-surface snow.

Corresponding author: Michael S. Town, michael.town@uib.no

Corresponding author: Hans Christian Steen-Larsen, hans.christian.steen-larsen@uib.no

21 Abstract

22 We document the isotopic evolution of near-surface snow at the EastGRIP ice core site
 23 in the Northeast Greenland National Park using a time-resolved array of 1-m deep iso-
 24 tope ($\delta^{18}O$, δD) profiles. The snow profiles were taken from May-August during the 2017-
 25 2019 summer seasons. An age-depth model was developed and applied to each profile
 26 mitigating the impacts of stratigraphic noise on isotope signals. There is a decrease in
 27 seasonal isotope-temperature sensitivity over 1.5 years of aging ($\Delta\delta^{18}O/\Delta T/\Delta t = 0.096 \pm 0.04$ ‰
 28 °C⁻¹·yr⁻¹). Isotopic changes *can* occur during summer seasons (increase in $\delta^{18}O$, de-
 29 crease in d-excess, d). After one year of aging the same summer layers always experience
 30 a 3-5 ‰ increase in d . Thus, d does not just carry information about source region con-
 31 ditions and transport history, but also integrates local conditions into summer snow lay-
 32 ers as the snow ages. No significant change is observed in $\delta^{18}O$ on interannual time scales.
 33 Isotopic-gradient-driven diffusion occurs throughout the year. It is most impactful in the
 34 summer seasons but does not explain all changes we observe. Other mechanisms of post-
 35 depositional processes are inferred to be net sublimation from surface and near-surface
 36 snow in summer seasons, and vapor-pressure-gradient driven exchange within the near-
 37 surface snow during shoulder seasons. Our results are dependent on the site character-
 38 istics (e.g. wind, temperature, accumulation rate), but indicate that more process-based
 39 research is necessary to understand water-isotope-to-climate proxies. Recommendation
 40 for monitoring and physical modeling are given, with special attention to the d-excess
 41 parameter.

42 Plain Language Summary

43 The relative abundance of heavy water isotopes have been used effectively to un-
 44 derstand the past climates of polar regions and beyond. Oxygen-18 in snow is thought
 45 to be a proxy for the local cloud or surface temperature. Deuterium excess, a derivative
 46 of heavy water isotopes, is considered an integrated history of water from source to de-
 47 position. We present data from a three-year study of near-surface snow at a polar ice
 48 core site in Northeast Greenland. Comparing annually successive samples of the same
 49 snow layers, we track changes in the snow after it is deposited. We date each snow layer
 50 to compare and average related layers. Net sublimation during summer sometimes en-
 51 riches the snow's oxygen-18, making it seem warmer than it actually was. Summertime
 52 sublimation also causes the deuterium excess to indicate that the snow came from closer

53 or more humid places. After a year or more of aging, summer snow layers nearly regain
54 their original deuterium excess signal. Open questions remain, and we recommend fu-
55 ture field work and modeling to investigate these questions. Highly-trained and observationally-
56 verified models can then be used to refine interpretation of polar ice cores.

57 1 Introduction

58 The relative concentration of stable water isotopes from polar snow and ice have
59 proven useful in telling warm from cold in reconstructions of Earth's past climate (e.g.,
60 Lorius et al., 1990; Jouzel et al., 1997; Johnsen et al., 2001; Jouzel et al., 2003; Kavanaugh
61 & Cuffey, 2003; Steig et al., 2013). In the past, climate reconstructions were dependent
62 on understanding the sensitivity of changes in water isotopes to changes in mean annual
63 temperature in the polar regions, i.e., the water-isotope-temperature sensitivity. Small
64 changes in this sensitivity had significant influence on inferences about past climates based
65 on polar ice cores (e.g., P. Grootes et al., 1993; Charles et al., 1994; Petit et al., 1999;
66 Jouzel et al., 2003). Recent climate reconstruction efforts are not as dependent on tem-
67 peratures inferred from water isotopes in polar snow, rather using an array of globally
68 distributed proxies (e.g., Rohling et al., 2012; Dahl-Jensen et al., 2013; Buizert et al.,
69 2021). However, simulation of past polar ice sheet mass balance and climate still require
70 accurate knowledge of ice sheet temperatures often derived from empirical isotope-temperature
71 sensitivities (e.g., Cuffey et al., 2016; Jones et al., 2023). Past circulation and weather
72 patterns are also possible to derive from combinations of isotope and other chemistry
73 measurements from polar snow and ice (e.g., Mayewski et al., 1994; Steffensen et al., 2008;
74 Guillevic et al., 2013; Jones et al., 2018). Such understanding is important not only to
75 make claims about past climate, but to improve models for prediction of weather and
76 future climate (e.g., Blossey et al., 2010; Werner et al., 2011; Dee et al., 2015; Dütsch
77 et al., 2019).

78 Despite the importance of accurate understanding the connection of isotope sig-
79 nals in polar snow and ice to climate, there is a lack of continuous understanding of how
80 climate is imprinted in the isotopic composition of polar snow, from moisture source to
81 eventual ice core extraction and analysis. Specifically, there is much to learn about what
82 happens to the isotopic signal in the top meter of snow when it is still under the influ-
83 ence of local meteorology. This study provides observations that document relevant meteorology-

84 induced isotopic changes in surface and near-surface snow that provokes a revised inter-
 85 pretation of the water isotope climate proxy.

86 1.1 Nomenclature

87 Here, we will use established nomenclature to discuss the concentration of heavy
 88 water isotopes in vapor, precipitation, or snow (Craig & Gordon, 1965; Dansgaard, 1964).
 89 Equation 1 shows the relative concentration of heavy water $H_2^{18}O$ to the more predom-
 90 inant lighter isotope (e.g., $H_2^{16}O$) in reference to the same isotopic ratio from a standard
 91 water source, the Vienna Standard Mean Ocean Water (VSMOW, Craig, 1961; Gonfi-
 92 antini, 1978).

$$\delta^{18}O = \left(\frac{\frac{H_2^{18}O}{H_2^{16}O}_{sample}}{\frac{H_2^{18}O}{H_2^{16}O}_{VSMOW}} - 1 \right) * 1000 \quad (1)$$

93 The water-isotope-temperature sensitivity is then defined as equation 2 for $\delta^{18}O$.

$$\gamma = \frac{\Delta\delta^{18}O}{\Delta T} \quad (2)$$

94 This relationship can be defined from either spatially-distributed data sets (i.e. γ_s),
 95 or temporally-derived data sets (i.e. γ_t). A linear pattern has been observed between spatially-
 96 distributed measurements of mean annual temperature and mean annual water isotope
 97 content of precipitation and surface snow, which we call γ_s (e.g. Dansgaard, 1964). Here
 98 ΔT usually represents the change in mean annual temperature associated with a change
 99 in $\delta^{18}O$ (i.e. $\Delta\delta^{18}O$). It has iteratively been realized that γ_s represents integrated
 100 temperature and distillation effects, as well as source region characteristics (Merlivat &
 101 Jouzel, 1979; Jouzel & Merlivat, 1984; Ciais & Jouzel, 1994). The water-isotope-temperature
 102 sensitivity can also be defined using observation- or model-based temporal variations of
 103 $\delta^{18}O$ and temperature for a location (e.g., γ_t , Cuffey et al., 1995, 2016; Werner et al.,
 104 2018). The temporal water-isotope-sensitivity, γ_t , is not necessarily the same as a γ_s for
 105 a similar region or climate.

106 Under equilibrium conditions, there is a linear pattern between $\delta^{18}O$ and the rel-
 107 ative concentration of deuterium-laden water, δD (Dansgaard, 1964). The intercept of
 108 this relationship is commonly referred to as 'deuterium excess' (d-excess or d , equation

109 3; e.g., Merlivat & Jouzel, 1979; Jouzel & Merlivat, 1984). It is used as an integrated char-
 110 acterization of an air mass’s water vapor and precipitation history. The mean value for
 111 equation 3 for global precipitation is 10 ‰ (Dansgaard, 1964). In polar snow, d is ex-
 112 pected to peak in Autumn precipitation and snow layers, and be a minimum in Spring
 113 precipitation and snow layers (Johnsen & White, 1989), influenced by sea ice extent, prox-
 114 imity to moisture source, and moisture source sea surface temperature. However, a sum-
 115 mertime peak in d has recently been observed in precipitation at Summit, Greenland (Kopeck
 116 et al., 2022).

$$d = \delta D - 8 * \delta^{18}O \quad (3)$$

117 Statistically, we are mainly concerned with how mean values compare even as dis-
 118 tributions of these isotopic values and their derivatives (i.e., $\delta^{18}O$ and d) may overlap.
 119 As such, most of our error values and uncertainty ranges are represented as two times
 120 the standard error around the means ($2\sigma_{\bar{x}}$, $p < 0.05$). Where the overlap of distribu-
 121 tions are important we report two times the standard deviation around the mean (i.e.,
 122 2σ).

123 When we discuss the influence of the near-surface atmosphere on the surface and
 124 near-surface snow, we will use the following definitions unless otherwise stated. The near-
 125 surface atmosphere is the atmospheric surface layer (e.g., Mahrt, 2014) where mechan-
 126 ical shear generates more turbulence than buoyancy generates or consumes. In the sta-
 127 ble boundary layers on polar ice sheets it can range from 10 m to 10s of meters thick de-
 128 pending on the inversion strength and wind speed (e.g., Hudson & Brandt, 2005; King
 129 & Turner, 2009). Operational definitions for surface snow and near-surface snow are 0-
 130 1 cm and 0-100 cm, respectively.

131 1.2 From source to sink

132 Isotope-enabled models (IEMs) of regional-to-global extent are now employed to
 133 probe complex relationships between water isotopes, including evaporative processes at
 134 the source, mixing and cloud physics processes along the way, and final precipitation physics
 135 (e.g., Blossey et al., 2010; Dee et al., 2015; Dütsch et al., 2019; Hu et al., 2022; Werner
 136 et al., 2011). Some focus is still on water-isotope-temperature relationships like γ_t (e.g.,
 137 Werner et al., 2018). Yet, it is recognized that a more comprehensive, process-based ap-

138 proach to isotope-climate relationships is necessary. The hydrologic cycle is then a pri-
139 mary focus of IEMs and their low-complexity predecessors (e.g., Merlivat & Jouzel, 1979;
140 Jouzel & Merlivat, 1984; Johnsen & White, 1989; Ciais & Jouzel, 1994; Blossey et al.,
141 2010; Werner et al., 2011). IEMs of a range of complexity have opened up nuanced, in-
142 tegrated interpretation of isotope concentration derivatives like d , advancing modeled
143 hydrologic processes and interpretation of ice cores (e.g. Merlivat & Jouzel, 1979; Jouzel
144 & Merlivat, 1984; Blossey et al., 2010; Dütsch et al., 2019; Hu et al., 2022).

145 **1.3 From sink to extraction**

146 After deposition at a polar site, the isotopic content of snow is not 'locked in place'
147 (e.g., Steen-Larsen et al., 2014), but continues to evolve in response to its surrounding
148 environment. Deeper in the firn and ice column (>2 m) and over longer time periods,
149 diffusion along isotopic gradients become a dominant smoothing process (Johnsen, 1977;
150 Johnsen et al., 2000; Gkinis et al., 2014; Jones et al., 2017). Proper inversion of this pro-
151 cess is necessary for accurate reconstruction of timing and magnitude of isotopic signals
152 (e.g., Johnsen et al., 2000; Vinther et al., 2010; Jones et al., 2018, 2023), although we
153 show here that additional isotopic corrections for surface and near-snow processes may
154 still be needed.

155 Reconstructions of past climates based on isotope signals in polar snow have his-
156 torically employed atmospheric IEMs coupled with isotopic-gradient smoothing inver-
157 sion methods (e.g., Steen-Larsen et al., 2011; Masson-Delmotte et al., 2015). These stud-
158 ies assume that no other processes influence the isotopic signal.

159 **1.4 The atmosphere-snow interface**

160 There is a growing body of literature demonstrating that local processes such as
161 wind-driven stratigraphy (Kochanski et al., 2018) and snow metamorphism (Colbeck,
162 1983) likely influence the isotopic content of surface (e.g., Münch et al., 2017; Wahl et
163 al., 2021, 2022) and near-surface snow (Town, Warren, et al., 2008; Steen-Larsen et al.,
164 2014; Casado et al., 2018; Madsen et al., 2019; Harris Stuart et al., 2023). It is uncon-
165 controversial to expect that post-depositional processes other than diffusion along isotopic
166 gradients might modify the isotopic content of near-surface snow (e.g. < 1 m). However,

167 we argue that there is little agreement on the mechanisms or net impact of post-depositional
168 change in seasonal or mean annual isotopic concentrations.

169 Modeling studies have shown that local meteorology can imprint near-surface at-
170 mospheric water vapor isotopic signals in the near-surface snow through forced-ventilation
171 (i.e., wind pumping) (Waddington et al., 2002; Neumann & Waddington, 2004; Town,
172 Warren, et al., 2008). Simulating the impacts of forced ventilation on snow requires time-
173 resolved knowledge of the surface snow structure, surface winds, accumulation rate, and
174 atmospheric and snow temperatures. Forced ventilation has been shown to potentially
175 smooth *and* bias isotope records after deposition. The potential isotopic bias occurs in
176 isotopically depleted winter layers during the relatively warmer summers at low accu-
177 mulation sites (Town, Warren, et al., 2008). Accurate isotope-based climate reconstruc-
178 tions from ice cores may depend sensitively on time-resolved knowledge of local mete-
179 orological conditions (e.g., accumulation and temperature) because a changing climate
180 may result in changing post-depositional biases Town, Warren, et al. (2008).

181 Observations confirm some results from the aforementioned modeling studies, but
182 also present more questions. At Dome Fuji, Antarctica, a cold and low accumulation ice
183 core site, there is a disconnect between the magnitude of the $\delta^{18}O$ annual cycle in pre-
184 cipitation and the firn (Fujita & Abe, 2006) that cannot be reconciled through inversion
185 of Johnsen et al. (2000) isotope-gradient-driven diffusion. Mechanical mixing of surface
186 snow also acts to smooth isotopic signals between precipitation layers. Horizontal av-
187 eraging across wind-induced snow structures (e.g. Filhol & Sturm, 2015) causes large vari-
188 ability in environmental signals (i.e. stratigraphic noise, e.g. Steffensen, 1985; Münch
189 et al., 2017; Zühr et al., 2021, 2023). The surface snow and near-surface vapor water iso-
190 topes co-vary on an hourly-to-daily basis during summer in Northern Greenland (Steen-
191 Larsen et al., 2014; Hughes et al., 2021; Wahl et al., 2021, 2022). Further observation
192 and laboratory studies have shown that sublimation can cause an isotopic enrichment
193 (Hughes et al., 2021).

194 Increased fidelity in surface and near-surface snow isotopologue observations have
195 led to improved models of the same. Observed changes in surface snow $\delta^{18}O$ at East-
196 GRIP has been successfully simulated by incorporating sublimation into an isotope-enabled
197 surface energy budget model (Wahl et al., 2022). Ritter et al. (2016) and Casado et al.
198 (2018) both employ elegant constrained models of the stable boundary layer. They ar-

199 gue that a thin layer of atmosphere over the Antarctic likely influences surface isotopic
200 content resulting in enrichment of surface $\delta^{18}O$ at the expense of $\delta^{18}O$ vapor in the sta-
201 ble boundary layer. Windier sites will likely have a well-mixed boundary layer, result-
202 ing in correlation between surface $\delta^{18}O$ content and overlying $\delta^{18}O$ vapor content (e.g.,
203 Steen-Larsen et al., 2014; Wahl et al., 2022). Casado et al. (2021) show evidence of post-
204 depositional change in surface snow induced by sublimation/deposition mechanisms, cit-
205 ing insolation and other surface energy budget processes as important to the surface $\delta^{18}O$
206 and d signals. At low accumulation sites scouring of annual layers is always a problem
207 to contend with (e.g., Epstein et al., 1965; Casado et al., 2018).

208 On the other hand, snow pit data from across East Antarctica, a range of climates
209 and accumulation rates, indicate that isotopic-gradient-driven diffusion, precipitation in-
210 termittency, and possibly spatial inhomogeneity may explain the signal to noise ratios
211 at these sites and further mechanisms are not necessary (Münch et al., 2017; Laepple et
212 al., 2018). At Summit Station, Greenland, Kopec et al. (2022) found very little post-depositional
213 change in isotopic content of precipitation after deposition, yet argue that sublimation
214 from the the Greenland ice sheet is responsible for the unique isotopic signatures observed
215 in the precipitation. This is consistent with the idea that Summit Station has a high ac-
216 cumulation rate (24 cm/year l.w.e.) mitigating post-depositional modification, albeit a
217 relatively warm mean annual temperature which would enhance post-depositional mod-
218 ification (Town, Warren, et al., 2008). Looking at one summer season at EastGRIP (Sum-
219 mer 2019), Zuhr et al. (2023) find evidence of local processes inducing post-depositional
220 change in d in snow down to 10 cm, with the repeatability and potential causes remain-
221 ing at large.

222 So, discrepancies in evidence and primary mechanisms of post-depositional mod-
223 ification of water isotope content of near-surface snow exist, inferred from both obser-
224 vations and models. Sublimation has already been shown to very likely the cause of ob-
225 served changes in the top 0.5 cm of snow, but what is happening below this depth while
226 the snow is still within the dynamic influence of the local atmosphere?

227 **1.5 This study**

228 To further quantitatively investigate the potential evolution of isotope signals be-
229 low the surface snow layer (0-1 cm), we present observations from a time-resolved study

230 of near-surface snow (0-100 cm) from the EastGRIP site in Northeast Greenland (Mojtabavi
 231 et al., 2020). Short snow cores (i.e. snow profiles) (80-100 cm in length) were taken at
 232 primarily biweekly frequency during summers (May - August) for the 2017, 2018, and
 233 2019 field seasons. Modeling indicates that significant change due to near-surface atmo-
 234 spheric influence is very unlikely below 1 m (Town, Warren, et al., 2008). The snow pro-
 235 files were taken during the summer seasons when one would expect meteorology-induced
 236 post-depositional processes to be strongest in near-surface snow. The snow profiles over-
 237 lap in depth from season-to-season, allowing a unique interannual look at the same snow
 238 layers. An age-depth model is developed for each individual snow profile to mitigate the
 239 impact of stratigraphic noise on grouping or averaging of isotope signals.

240 We will demonstrate that while there is inconsistent post-depositional modifica-
 241 tion of $\delta^{18}O$ during the summers and interannually, d shows more consistent modifica-
 242 tion in summer snow layers on weekly and interannual timescales. We explore the po-
 243 tential mechanisms causing these signals and implications of these results for future in-
 244 terpretations of d in polar snow, firn, and ice.

245 **2 Site Description, Data, and Methods**

246 The data and products presented here are all derived from observations at the East-
 247 GRIP ice core site located in the Northeast Greenland National Park. In Section 2.1 we
 248 present the meteorological context of our study. In Section 2.2 and Section 2.3 we present
 249 the surface snow isotope and snow profile isotope data sets, respectively. In Section 2.3.1,
 250 we explain the siting, extraction, handling, and processing of the snow profiles. In Sec-
 251 tion 2.4, we discuss the age-depth model applied to the snow profile isotope data set. In
 252 Section 2.5 we discuss nuances and caveats relevant to the interpretation of the data pre-
 253 sented here. Table 1 contains an overview of the data used in this study.

254 **2.1 Meteorology: data and context**

255 The EastGRIP site sits at $75^{\circ}37'47''N$, $35^{\circ}59'22''W$, with an altitude of 2708 m (Mojtabavi
 256 et al., 2020), on fast moving ice stream (55 m/year Westhoff et al., 2022). There is a PROMICE
 257 weather station (Fausto et al., 2021) located approximately 300 m south of our study
 258 site. The site experiences a persistently high and directionally constant winds because
 259 its location on the ice sheet results in downslope (westerly) katabatic winds and west-

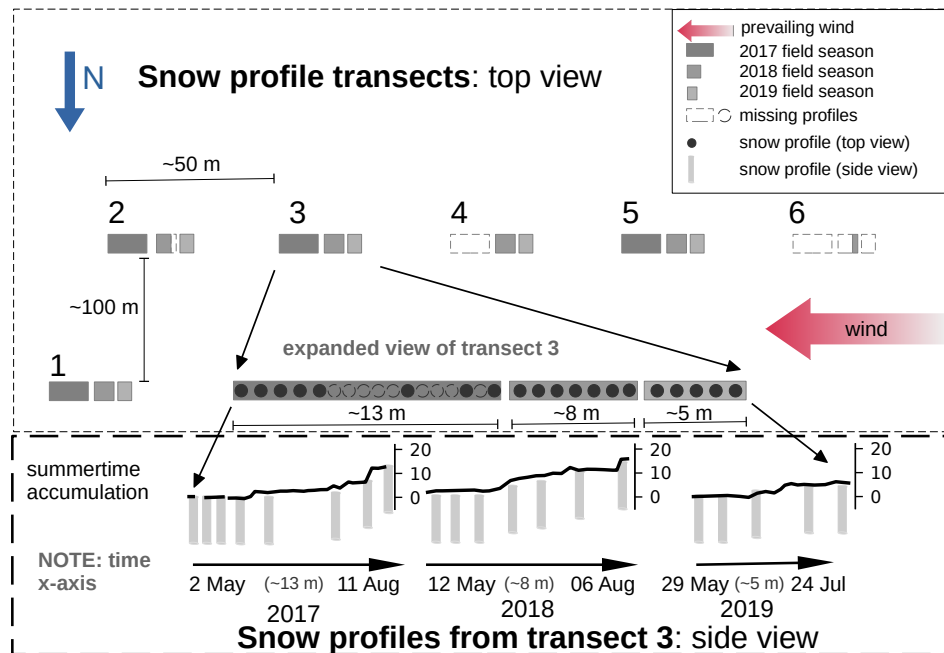


Figure 1: The top panel shows an overview of the relative spacing and timing of the transects along which the near-surface snow profiles were taken for this study. Each transect has the same snow profile pattern as illustrated in the expanded view of transect 3, a representative transect. The diagram is not to scale, but distances are noted. North is downward in this diagram. The prevailing wind direction is from the W-SW. The number and relative timing of snow profiles are accurately indicated. The bottom panel shows an illustration of the summertime accumulation along with snow profile timing. The study site is the EastGRIP ice core site in Northeast Greenland.

260 erly synoptic flow over the ice sheet (Putnins, 1970). See Table 1 for meteorology data
261 summary.

262 The accumulation rate was measured as approximately 134-157 mm/year of liq-
263 uid water equivalent (l.w.e.) from snow pit studies coincident with this work (Nakazawa
264 et al., 2021; Komuro et al., 2021). Summertime daily accumulation was measured with
265 stake lines during the 2016-2019 field seasons (Steen-Larsen, 2020a, 2020b; Harris Stu-
266 art et al., 2023). The stake line was 200-m long with 1-m spatial resolution in the 2016
267 field season, and 90-m long with 10-m spatial resolution for the remaining field seasons.
268 We also determined changes in monthly mean snow height from PROMICE sonic ranger
269 data (Fausto et al., 2021) for 2014-2019, with the annual snow accumulation rate being
270 approximately 40 cm/year. The top 1-m of snow has a nearly constant density profile
271 of approximately 337 kg/m^3 , presumably constant because of the persistently high winds
272 at EastGRIP (Schaller et al., 2016; Nakazawa et al., 2021; Komuro et al., 2021). The snow
273 surface is spatially heterogeneous in height, with surface features smoothing slightly through-
274 out the summer seasons (Zuhr et al., 2021, 2023).

275 2.2 Surface snow isotopes

276 The top 0-1 cm snow was collected along a 1000 m wind-parallel path in the 2016
277 field season, and a 100 m path for the 2017-2019 field seasons (Hörhold et al., 2023; Hörhold,
278 Behrens, Hoffmann, et al., 2022; Hörhold et al., 2022; Hörhold, Behrens, Wahl, et al.,
279 2022). During the 2016 and 2017 field seasons, samples from each site were collected and
280 bagged individually, the measured $\delta^{18}\text{O}$ then averaged. During the 2017 field season, snow
281 of equal amounts was also collected daily at the same locations then mixed into one sam-
282 ple bag. These were termed 'consolidated' samples. It was found from this work that the
283 mean isotopic values of the individually bagged samples were the same as the less labo-
284 riously obtained 'consolidated' samples. Mean daily surface snow isotopic content for the
285 summers of 2018 and 2019 were therefore determined from 'consolidated' samples.

286 Once collected, either individually or as a consolidated sample, the snow was sealed
287 in an air-tight Whirl-Pak bag and kept frozen until measurement at the Alfred-Wegener-
288 Institut in Bremerhaven, Germany. Isotopic measurement procedures for surface snow
289 are the same as for the snow profiles. See Section 2.3 for details.

2.3 Near-surface snow profile isotopes

2.3.1 Snow profiles: siting, extraction, handling, and measurement

The central data presented here are isotope measurements from a time-resolved array of 1-m near-surface snow profiles. See Figure 1 for a visualization of the snow profile sampling strategy. The snow profiles were taken along a transect progressing in the windward direction. On each sample date 4-5 snow profiles were taken, each one from a unique transect line. All profiles were extracted within a few hours of each other. The transect lines are spaced out by at least 50 m. We consider them independent representations of the near-surface snow as they are out of the range of isotopic spatial autocorrelation (Münch et al., 2016).

Snow profile locations along each transect were taken between three and twenty-one days apart, the most common sampling frequency being fourteen days. They were spaced apart by approximately one meter from sampling event to sampling event. Profiles taken along one track and adjacent in time are then considered to represent the same snow. These profiles are still susceptible to stratigraphic noise documented by Zuhr et al. (2023). A single profile was taken by gently pushing a 10-cm diameter carbon fiber tube (i.e. liner) with a 1-mm thick wall into the snow. Minimal compression of the snow column occurs during this process (maximum 2 cm, average 1 cm, Section 2.1 in Schaller et al., 2016). A small pit was cleared on the downwind side of the tube so that the liners could be carefully extracted with all snow. The resulting snow pit was then back-filled within two hours of the beginning of the process.

After extraction, each profile was quickly transported to a cold tent for cutting and storage. The profiles were cut at 1.1-cm resolution for the top 0-10 cm and 2.2-cm resolution for remainder of the profiles. Most profiles were not exactly 100 cm due to compression and a small amount of loss from the bottom of each profile. The snow was cut in an open-faced core tray using a 0.10-cm thick blade. Each sample was sealed in an air-tight Whirl-Pak bag and kept frozen until measurement at either the Alfred-Wegener-Institut in Bremerhaven, Deutschland or the Institute of Earth Sciences in Reykjavík, Island.

Measurements of $\delta^{18}O$ and δD concentrations were done using a Picarro cavity ring-down spectrometer (models L2120-i, L2130-i, L2140-i) and reported in per mil (‰) no-

321 tation as shown in equation 1 on the VSMOW/SLAP scale. Memory and drift correc-
 322 tions were applied using the procedure in (Van Geldern & Barth, 2012). The combined
 323 1σ uncertainty in $\delta^{18}O$ is 0.11‰ and for δD is 0.8‰ for all isotopic measurements. We
 324 calculated the combined standard uncertainty (Magnusson et al., 2017) including the long-
 325 term uncertainty and bias of our laboratory by measuring a quality check standard in
 326 each measurement run and including the uncertainty of the certified standards.

327 **2.4 Intercomparison of chronological layers**

328 **2.4.1 Depth correction**

329 At EastGRIP, the uneven surface and concomitant heterogeneous distribution of
 330 precipitation results in spatially heterogeneous isotopic concentrations of snow (Zuhr et
 331 al., 2023). A perfectly horizontal average of $\delta^{18}O$ in snow then represents a mixture of
 332 events across time (Münch et al., 2017). Zuhr et al. (2023) estimates that the 2σ spread
 333 around mean $\delta^{18}O$ values as a function of depth is 2.9‰ due to the impact of this strati-
 334 graphic noise. For this study, tracking chronological layers is critical so that wind-driven
 335 spatial heterogeneity in $\delta^{18}O$ is separated from other processes at work in the near-surface
 336 snow.

337 We applied a local depth correction to individual snow profiles to better compare
 338 chronological layers. Photogrammetric experiments at EastGRIP show that chronolog-
 339 ical layers of snow are inhomogeneous in thickness and spatial distribution (Zuhr et al.,
 340 2021), in agreement with prior efforts documenting wind-driven erosion and deposition
 341 in snow (e.g., Fisher et al., 1985; Colbeck, 1989; Filhol & Sturm, 2015). Important pre-
 342 cipitation events will have uneven representation in the snow, and in extreme cases (high
 343 winds with low accumulation) entire annual layers could be scoured (e.g., Epstein et al.,
 344 1965; Casado et al., 2018).

345 For the 2017 snow profiles, we apply one depth correction to all profiles collected
 346 on one day. We use the mean change in height from the 200-m snow stake transect to
 347 adjust snow surface height relative to the first profiles of the season collected on 2 May
 348 2017 (?). We tracked changes in surface height along individual transects for the 2018
 349 and 2019 seasons.

350 **2.4.2 Age-depth model**

351 The depth correction mitigates much of the stratigraphic noise induced by simple
 352 horizontal averaging, but not all. We developed an age-depth model for each individual
 353 snow profile to improve mitigation of stratigraphic noise on chronological layer intercom-
 354 parison.

355 An illustration of the age-depth model process is shown in Figure 2. The end date
 356 for every profile is the extraction date. From this date we worked downwards in the snow
 357 and backwards in time, local maximum and minimum $\delta^{18}O$ values were found automat-
 358 ically. Dates were assigned to the $\delta^{18}O$ values are from the nearest maxima and min-
 359 ima in monthly mean temperature as measured at the nearby PROMICE weather sta-
 360 tion. We find at least two dates per annual layer.

361 The exact date assigned to each assignment for peak $\delta^{18}O$ and monthly mean tem-
 362 peratures was 31 July. Maximum temperatures occur consistently during mid-July at
 363 EastGRIP. Maxima in $\delta^{18}O$ have been observed to trail temperature maxima by as much
 364 as a month at EastGRIP (Harris Stuart et al., 2023) likely due to post-depositional sub-
 365 limation, similar to Dome C, Antarctica (Casado et al., 2018) - a much lower accumu-
 366 lation site. The date assigned for the wintertime $\delta^{18}O$ minima was the first of each month.
 367 The Greenland Ice Sheet can experience moderately coreless winters (Putnins, 1970). So,
 368 the winter month with the minimum mean temperature may be one of a range of months
 369 (December-April).

370 The uncertainty in the age-depth model comes from a combination of the uncer-
 371 tainty in snow profile depth values and uncertainty in dates assigned to each $\delta^{18}O$ max-
 372 ima or minima. Examining only uncertainty from the snow profile resolution, we assume
 373 that choice of the $\delta^{18}O$ maxima/minima values might be off by as much as one depth
 374 level in the snow profile. This is an error of ± 1 cm for the top 10 cm of each profile and
 375 ± 2 cm for the rest of each profile. If the accumulation rate is 40 cm/year then the re-
 376 sulting uncertainty in age-depth is approximately ± 9 for the top 10 cm and ± 18 days
 377 for the rest each profile.

378 We estimate the uncertainty in date assignment separately for Summer and Win-
 379 ter. Peak summer temperatures at EastGRIP consistently occur during the middle of
 380 July. Thus, the uncertainty in 31 July date assigned to peak $\delta^{18}O$ values is ± 7 days.

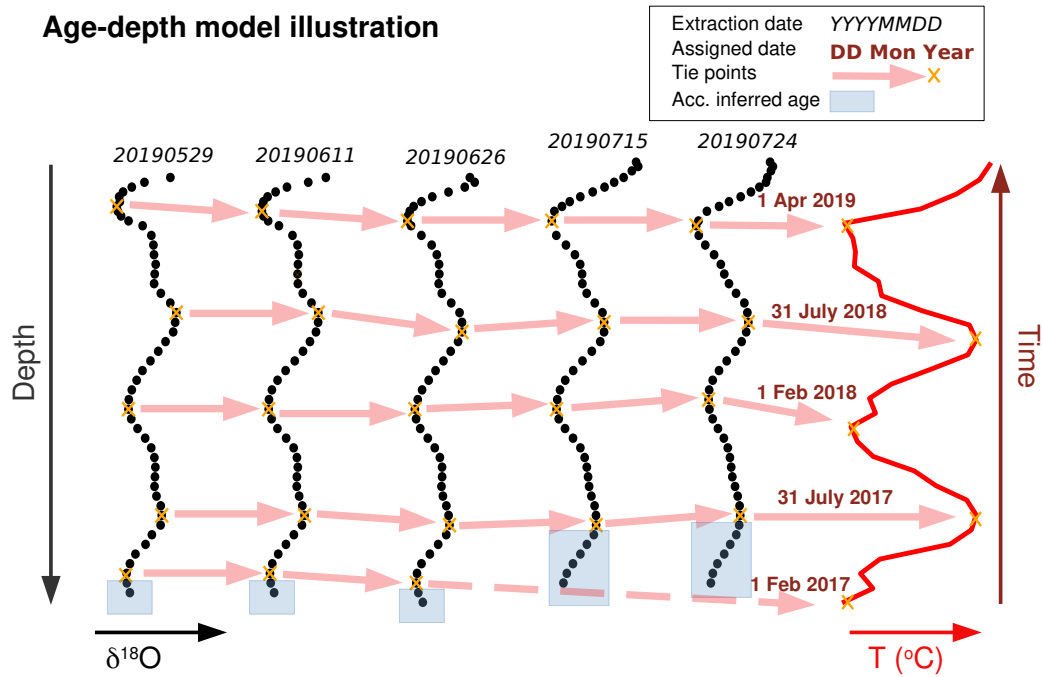


Figure 2: An illustration of the age-depth model applied to $\delta^{18}O$ data from transect 2 during the 2019 field season. The yellow stars represent automatically found peaks in $\delta^{18}O$ (black dots) and monthly mean 2-m temperature (red line). Each yellow star is assigned a date, and the intervening dates are linearly interpolated to a depth value. The lowest few $\delta^{18}O$ data points are assigned by an iterative process based on accumulation rate and manually checked. See text for details.

381 The coldest month in any winter may range from December to April (Putnins, 1970).
 382 Precipitation does not likely come during the minimum temperatures. The minimum $\delta^{18}O$
 383 values then represent the coldest precipitation events. We assume that these coldest pre-
 384 cipitation events happen during the coldest months. We know which months are cold-
 385 est, but assigning a date to the coldest precipitation events overreaches the power of our
 386 meteorology data. So, we set the date for minimum $\delta^{18}O$ values to the first of each cold-
 387 est month, acknowledging that we might be off by as much as ± 30 days.

388 Taken in total, we conservatively assess the 2σ uncertainty of each summertime date
 389 assignment as ± 25 days, and the uncertainty of each wintertime date assignment as ± 48
 390 days. The accumulation rate at EastGRIP is not constant, with higher rates in Summer
 391 and Autumn than Winter and Spring. From the PROMICE sonic ranger data, approx-
 392 imately 50% of the accumulation comes from 20% of the events (Fausto et al., 2021). Dur-
 393 ing high accumulation rate time periods, the dating uncertainty will be much smaller,
 394 and vice versa.

395 Figure 2 represents a transect in which the age-depth model did not vary much from
 396 profile-to-profile. In this case, the depth correction provided a strong start for the age-
 397 depth model. The age-depth model varies more between snow profiles taken during the
 398 2017 season when the depth correction was not as strong. Evidence for this can be seen
 399 in the dramatic difference in uncertainty around the 2017 mean profiles between Figure
 400 3(a) and Figure 3(c).

401 The age-depth model is reliable when clear $\delta^{18}O$ maxima and minima exist in the
 402 snow profiles, which is true for the vast majority of each profile. The exceptions are sys-
 403 tematically at the bottom of each snow profile. Rarely did the bottom of any core end
 404 in a clear maxima or minima, so a different procedure was developed for these occurrences.
 405 First we use the earliest date assigned (i.e. deepest maxima or minima) in the profile to
 406 estimate the remaining snow left undated. We then iteratively found the mean accumu-
 407 lation rate for this remaining snow by assuming a mean accumulation rate of 40 cm/year
 408 to frame the appropriate time period then determining the mean accumulation rate for
 409 the correct time period using the sonic ranger data set from Fausto et al. (2021). The
 410 age-depth model for the bottom of the profile is the inverse of the mean accumulation
 411 rate. Finally, we assessed the resulting $\delta^{18}O$ profile against the entire data set. Profiles
 412 with dramatically different age-depth models at the bottom were assigned a starting date

413 to match their $\delta^{18}O$ values with seasonally appropriate times. Between 10-20% of each
414 profile will have received the accumulation-rate-informed age-depth model.

415 **2.5 Nuances and caveats in the snow isotope data set**

416 ***2.5.1 Decorrelation distances and snow profile comparisons***

417 Our sampling strategy is designed to separate spatial and temporal variability of
418 isotopic content of the near-surface snow. The sampling strategy is inherently destruc-
419 tive. This results in trade-offs between accurate sampling and monitoring temporal vari-
420 ability. The transects shown in Figure 1 observe the same location as much as possible
421 by sampling at approximately 1-m spacing along each transect. The 1-m spacing keeps
422 each profile well within established spatial decorrelation distances for spatially succes-
423 sive water isotope samples (1.5 m) in similar climates (Münch et al., 2016). We did not
424 sample much closer than 1-m to leave the next sample relatively undisturbed. This last
425 point is further explored in the next section (Section 2.5.2).

426 The decorrelation distances derived in Münch et al. (2016) were done so without
427 application of spatial depth adjustment or an age-depth model to align chronological lay-
428 ers. They thus represents extreme decorrelation distances for our data set. We expect
429 our decorrelation distances to be slightly higher after the application of depth adjust-
430 ments, and much higher after application of our age-depth model.

431 While each transect line is intended to represent the same snow, during 2017 many
432 (18) profiles were taken along each transect although not all used here (only 8). Even
433 considering the enhanced autocorrelation of samples because of our age-depth model, it
434 is very likely that the snow extracted from a transect at the beginning of the 2017 sea-
435 son does not represent the same location as the snow from the end of the 2017 season
436 along the same transect. We consider this later when examining intraseasonal evolution
437 of the near-surface snow.

438 The transect lines are separated by 50 m or more to provide 'independent' repre-
439 sentations of the snow surface. Several dune and sastrugi features will manifest in these
440 distances (Zuhr et al., 2021), making each of these transects independent as far as pre-
441 cipitation and wind-driven surface features are concerned.

442 ***2.5.2 Mitigated biases due to sampling***

443 The combination of a 1-m distance between each profile along one transect along
444 with prompt back-filling of each extraction mitigates the influence of near-surface me-
445 teorology on the next upwind profile. High temperature gradients take days to weeks to
446 propagate through the snow these distances (Town, Waddington, et al., 2008). The po-
447 tential influence of force ventilation on near-surface snow due to tapers off dramatically
448 after about 50 cm (Town, Warren, et al., 2008). So, our sampling procedure prevents un-
449 intended post-depositional change due to extra exposure to the near-surface atmosphere.

450 ***2.5.3 Missing data and other sources of uncertainty***

451 Transect line 4 was impacted by traffic or resampling during the 2017 field season.
452 It was left out of these analysis. Transect lines 2-5 were shifted inadvertently up one tran-
453 sect in the middle of the 2018 field season due to a change in field personnel. This was
454 corrected during post-processing.

455 In addition to the 1-m profiles used here, nine shorter profiles (30 cm in length) were
456 taken in 2017. We do not use these data here as they do not provide interannual infor-
457 mation. The shorter profiles nevertheless represent distance traveled along each tran-
458 sect. For the short profiles, the spacing between profiles was smaller, approximately 50
459 cm. So, the total distance traveled along the 2017 transects is estimated as a conserva-
460 tive 13 m.

461 Compression often occurred during the extraction of the snow. Standard procedure
462 would be to apply a correction for this compression evenly across each profile, partic-
463 ularly in deeper firn or ice. However, we believe that the location of compression is more
464 likely localized in near-surface snow. In a 1-m snow profile from this site, there are least
465 five locations where the compression might have occurred, at the surface or the Spring
466 or Autumn hoar layers. It is also certain that the compression did not occur evenly across
467 any profile. The compression values are small relative to the profile lengths and iden-
468 tifying the hoar layers after extraction is tricky. So, we leave the compression amount
469 as an effective uncertainty in the dating, a probable maximum value of 9 days.

470 Finally, we did not adequately assess the relative starting heights of the transects
471 at the beginning of each season. This induces relative errors of around 3-5 cm in our depth

472 adjustment between each snow profile based on May surface roughness estimates from
473 (Zuhr et al., 2021). The missing information does not impact the age-depth model.

474 **3 Results**

475 The snow sampling strategy employed here is designed to provide successive sea-
476 sonal and interannual looks at snow layers to track any post-depositional isotopic changes
477 as the snow ages. The surface snow data (0-1 cm) is only from summer. It is not pre-
478 cipitation, but provides an immediate context for the isotopic content of recent snow ac-
479 cumulation. The near-surface snow (0-100 cm) we characterize with annually returning,
480 closely-spaced snow profiles along distributed transects. This strategy allows snow pro-
481 files to be meaningfully intercompared on a weekly-to-biweekly basis throughout a sum-
482 mer season. The sample depth ensures that we have measured past the lower boundary
483 of any potential influence of the near-surface atmosphere (e.g., Waddington et al., 2002;
484 Town, Warren, et al., 2008), and provides successive looks at the same snow layers as
485 they age from year-to-year. The interannual data are presented in Section 3.1 and summer-
486 only data are presented in Section 3.2. The implications of these results and future work
487 are discussed in Section 4.

488 **3.1 Interannual variability and evolution**

489 Figures 3 and 4 show annually successive surface and near-surface snow isotopic
490 content for $\delta^{18}O$ and d , respectively. The dates represented by the snow span 2014-2019.
491 The age of the snow may range from two to three years depending on the extraction date.
492 Figures 3(a) and 4(a) show the mean profiles with $2\sigma_{\bar{x}}$ shading around each mean. The
493 data are plotted against relative depth with 0 m chosen as 29 May 2019, the day of the
494 first snow profile during the 2019 summer field season. Figures 3(b) and 4(b) show the
495 difference between each profile as a function of relative depth. These difference profiles
496 represent the isotopic change due to aging in the firn.

497 As stated in Section 2.4, we have mitigated the impact of stratigraphic spatial in-
498 homogeneity on horizontal averaging (Figures 3(a,c) and 4(a,c)). For the 2017 profiles,
499 we apply the same depth correction to all snow profiles as individual surface height track-
500 ing was not possible. This results in larger $2\sigma_{\bar{x}}$ shading around the 2017 mean snow pro-
501 files.

502 Figures 3(c,d) and 4(c,d) show the same isotopic data as in their respective pan-
 503 els (a,b), but now against the age-depth model described in Section 2.4. The age-depth
 504 model better aligns chronological layers than the accumulation adjustments, further mit-
 505 igating deleterious impacts of spatial inhomogeneity in stratigraphy and densification on
 506 quantitative comparison $\delta^{18}O$ and d in snow layers. This can be seen in a decrease $2\sigma_{\bar{x}}$
 507 values from panel (a) to panel (c) in Figures 3 and 4, particularly for the 2017 snow pro-
 508 files. Although accumulation is fairly continuous at EastGRIP (Fausto et al., 2021), more
 509 accumulation comes in the Summer and Autumn over Winter and Spring. This weight-
 510 ing difference weighting explains the differences between Figures 3(b)/4(b) and 3(d)/4(d).

511 Figure 5 shows the difference between annually successive mean snow profiles. It
 512 is similar to panel (d) from Figures 3(c,d) and 4 but with $2\sigma_{\bar{x}}$ shading. Figure 5 can be
 513 interpreted as how $\delta^{18}O$ and d evolve one or two years after being interred, now as a func-
 514 tion of reference snow profile age.

515 Annual and seasonal statistics from Figures 3, 4, and 5 are shown in Tables A1-
 516 A4 in Appendix A.

517 **3.1.1 Interannual evolution of $\delta^{18}O$**

518 Mean annual $\delta^{18}O$ values are fairly constant throughout this time period regard-
 519 less of aging, approximately -36 ‰ . However, there is significant variability in the peak
 520 summer $\delta^{18}O$ in each profile, regardless of snow age. The 2019 summer has the great-
 521 est peak $\delta^{18}O$ values. There is not concomitant variability in the minimum winter $\delta^{18}O$
 522 values in this record. Some differences between profiles seem significant when plotted against
 523 relative depth. However, when the age-depth model is applied, differences between pro-
 524 files show no significant interannual change in $\delta^{18}O$ (Figures 3(d) and 5(a)).

525 We compute a seasonal temperature sensitivity (γ_t) using minimum (winter) and
 526 maximum (summer) $\delta^{18}O$ values with corresponding minimum and maximum monthly
 527 mean temperatures, using the same tie points as those used in the development of the
 528 age-depth model (Figure 2). This is similar to subseasonal temperature sensitivities found
 529 in Greenland (e.g., Shuman et al., 1995; Bolzan & Pohjola, 2000) and the Antarctic (e.g.,
 530 Casado et al., 2018). We find γ_t for each half year by using the ratio of seasonal change
 531 (summer-to-winter, winter-to-summer) in $\delta^{18}O$ over the seasonal change in monthly mean
 532 temperature. We find a mean γ_t that starts at approximately $0.297 \pm 0.03 \text{ ‰} \cdot \text{°C}^{-1}$ and

533 decreases at a rate of $0.096 \pm 0.04 \text{‰} \cdot \text{°C}^{-1} \cdot \text{year}^{-1}$. We have chosen to fit a linear pat-
 534 tern, but there could be a more dramatic drop in γ_t over the first 0.5 years then a much
 535 slower change in γ_t thereafter. More data and modeling are necessary to probe this re-
 536 lationship for EastGRIP.

537 During the season of extraction, the surface snow $\delta^{18}\text{O}$ values (purple squares) and
 538 mean summer snow profile $\delta^{18}\text{O}$ values match in mean and approximate variability for
 539 this record. After aging one year, the mean snow profile $\delta^{18}\text{O}$ for July 2018 extracted
 540 in 2019 matches the mean surface snow $\delta^{18}\text{O}$. However, the surface snow $\delta^{18}\text{O}$ from 2016
 541 and 2017 are several per mille enriched over the snow that has aged one or two years.

542 Using the summer $\delta^{18}\text{O}$ profile peaks as annual markers, we find a mean annual
 543 accumulation rate of $45.6 \pm 3.8 \text{ cm}$ ($13.5 \pm 1.1 \text{ cm/year l.w.e.}$) for this time period. This
 544 is consistent with accumulation rates for EastGRIP just prior to the observation period
 545 with a similar method (Nakazawa et al., 2021; Komuro et al., 2021), as well as coinci-
 546 dent estimates from PROMICE sonic rangiers (Fausto et al., 2021).

547 *3.1.2 Interannual evolution of deuterium excess*

548 Figure 4 shows the interannual variability of deuterium excess (d). Clear seasonal
 549 cycles are shown on both depth and age-depth scales. The minima occur during the Spring
 550 and Summer, while the maxima occur during Autumn as one might expect from Johnsen
 551 and White (1989), but in variance with Kopec et al. (2022). There are significant dif-
 552 ferences between the summer d values from surface snow and the snow profiles during
 553 the season of extraction. The mean summer surface snow d is 8-10 ‰, whereas the mean
 554 snow profiles show d values of only a 3 and 5 ‰ in 2018 and 2019, respectively. This
 555 is similar to what was found by Zuhr et al. (2023) for summer 2019 at EastGRIP. In 2017,
 556 we see higher mean d in the summer snow profiles just after deposition, but still less than
 557 in the mean surface snow d (See Table A5). The surface snow has a large range in d val-
 558 ues as synoptic events bring in high d precipitation, followed by periods of decreases in
 559 d due to sublimation (Harris Stuart et al., 2023). The evolution of the near-surface snow
 560 during the summer field seasons is discussed in greater depth in Section 3.2 and Section 4.

561 The differences between d profiles shows a distinct pattern peaking during the sum-
 562 mer layers (Figures 4(d) and 5(b)). The surface summer snow starts with a relatively
 563 high d value that decreases by as much as 5 ‰ by the time it is extracted as a snow

564 profile. After aging for one or two years, the same summer layer d have increased up to
 565 5 ‰ because the Autumn maximum peaks broaden into Summer and Spring layers. Al-
 566 though not rising to the level of $2\sigma_{\bar{x}}$ significance, there is also a persistent decrease in win-
 567 ter d values shown in Figure 4(d) as the snow ages interannually. The mean annual val-
 568 ues of d do not change from year-to-year, regardless of aging (Table A3).

569 3.2 Summer evolution of $\delta^{18}\text{O}$ and d

570 Figure 6 provides a look at the isotopic evolution of the near-surface snow during
 571 the summer field seasons. The extraction dates (upward arrows), 2-m air temperature,
 572 and accumulation from bamboo stake field are provided for context. Some spatial vari-
 573 ability is no doubt represented in contour plots as temporal variability although snow
 574 profiles along one transect were nearly coincident in space and corrected for changes in
 575 surface height (Figures 6(d-i)). Each upward arrow represents the mean of 4-5 snow pro-
 576 files from different transects. The spatial variability is likely averaged out by grouping
 577 of snow profiles from different transects.

578 We show little more than the first annual cycle (0-50 cm) because there is no de-
 579 tectable subseasonal change below approximately 20-30 cm. However, the top 10-15 cm
 580 of snow shows important evolution responding to both influxes of new accumulation and
 581 impacts of sublimation during periods of high temperatures and low-to-no accumulation.
 582 New accumulation can bring in a range of $\delta^{18}\text{O}$ values, but typically has a high ($\geq 10 \text{ ‰}$)
 583 d content. During periods of low-to-no accumulation there are coincident increases in
 584 $\delta^{18}\text{O}$ and decreases in d . This is a known signal of sublimation (Hughes et al., 2021; Wahl
 585 et al., 2022; Harris Stuart et al., 2023), yet the patterns could be a result of spatial in-
 586 homogeneity represented as temporal evolution. We find this unlikely due to the con-
 587 sistency with which sublimation signals happen during low-to-no accumulation using time
 588 as the x-axis perspective. Further, low-to-no accumulation periods do not show other
 589 combinations of changes in $\delta^{18}\text{O}$ and d , and each contour plot represents an average across
 590 spatially distant transects.

591 Figures 7-9 illustrate the changes in mean daily profiles from two dates from the
 592 middle of each summer during low-to-no accumulation. Significant increases ($p < 0.05$)
 593 in $\delta^{18}\text{O}$ are seen the summers of 2017 and 2019, down to 10-15 cm. Coincident decreases
 594 in d are also seen in these difference plots, but not to $p < 0.05$. Temporal changes in

595 the 2018 snow profiles are not so easily encapsulated in a profile difference plot shown.
 596 In this case there is no significant change in $\delta^{18}O$ and d over the chosen low-to-no ac-
 597 cumulation period. Other periods during 2018 may show significant differences in their
 598 profiles, but we choose here to keep the time periods as similar as possible for this illus-
 599 tration.

600 Nevertheless, across the 2018 and 2019 summer seasons we see a 5 ‰ difference
 601 in d from when it is sampled at the surface and when it is extracted as a snow profile
 602 in the same summer. This difference is not apparent in the 2017 summer data. See
 603 Figure 4(d) and Table A5 in the Appendix.

604 4 Discussion

605 There are significant changes in the isotopic content of near-surface snow after de-
 606 position at the EastGRIP site. We observe these changes happening on two timescales,
 607 during the summer season and interannually. The largest changes we observe are in the
 608 summer snow layers on both timescales. Enrichment in $\delta^{18}O$ and a decrease in d can hap-
 609 pen during the summer season in the top 10-15 cm of snow during low-to-no accumu-
 610 lation periods. A subsequent increase in the summer snow layer d occurs as the snow ages
 611 one or two years in the firn. Below we discuss potential mechanisms for these processes,
 612 their implications, and make recommendations for future work.

613 4.1 Mechanisms of post-depositional processes at EastGRIP

614 The factors that combine to change isotopic content of near-surface snow are: el-
 615 evated air and snow temperatures, air and snow temperature gradients, absolute humid-
 616 ity levels, air and snow humidity gradients, near-surface wind speeds, surface structure,
 617 snow density, accumulation rate, and redistribution (scouring and filling) of snow. As
 618 an observational effort, inferences we make about potential mechanisms necessarily re-
 619 quire further study, recommendations for which we make in Section 4.2. Nevertheless,
 620 some strong inferences can be made through context and compositing of the results from
 621 Section 3.

622 **4.1.1 Summer**

623 As stated in Section 3.2, the change in near-surface $\delta^{18}O$ and d that occurs dur-
 624 ing summer can have a sublimation signature, increase in $\delta^{18}O$ and decrease in d , dur-
 625 ing low-to-no accumulation events. This has also been observed and modeled at East-
 626 GRIP in surface snow (Wahl et al., 2022). Similar patterns of isotopic change were ob-
 627 served in a higher resolution, vertically and horizontally, summertime data set for East-
 628 GRIP down to 30 cm (Zuhr et al., 2023).

629 The mean surface snow d in this data set is almost always greater than the snow
 630 profile d that has aged a few days or weeks (Figure 4(c)), which is a likely sublimation
 631 signal. However, there is not proportional enrichment of $\delta^{18}O$ when comparing surface
 632 snow to snow profiles (Figure 3(c)). The isotopic changes we see in our case studies (Fig-
 633 ures 7-9) do not always rise to the level of $2\sigma_x$ significance, likely induced by spatial in-
 634 homogeneity. Clear patterns related to possible post-depositional modification do seem
 635 present when looking at the summers as a whole (Figure 6).

636 Exploring possible mechanisms for the clear differences we see in d between sur-
 637 face snow and near-surface snow, as well as the patterns shown in Figure 6, we first as-
 638 sess isotopic gradient diffusion (Johnsen et al., 2000). Using Johnsen et al. (2000) isotopic-
 639 gradient-driven diffusion under extreme conditions (i.e. the steepest mean isotopic gra-
 640 dients, warm summer temperatures $-11\text{ }^\circ\text{C}$ for 60 days), there can be a change in $\delta^{18}O$
 641 of up to $2\text{ }^\circ\text{‰}$. We observe in our snow profiles changes much larger than $2\text{ }^\circ\text{‰}$ over 47
 642 days in 2017 (Figure 7(a)). We are not observing a pure isotopic-gradient diffusion sit-
 643 uation because the real snow surface is open to the atmosphere, its isotopic content fluc-
 644 tuating on many time scales. Casado et al. (2021) show that summer surface snow $\delta^{18}O$
 645 at Dome C, Antarctica responds to more than surface temperature, with sublimation and
 646 deposition being important aspects to simulating isotope observations.

647 The Johnsen et al. (2000) diffusion also has a smoothing effect, but we also observe
 648 biases induced in the surface and near-surface snow. A change in mean isotopic content
 649 over a shallow, near-surface layer implies the influence of the near-surface atmosphere.
 650 To substantiate this inference, we simulate interstitial air flow with a model of wind-pumping
 651 in snow (Colbeck, 1997). We use mild surface topography and mean wind conditions (rolling
 652 dunes, $\lambda = 0.5\text{ m}$, $h = 0.25\text{ m}$; $\rho_{snow} = 350\text{ kg/m}^3$; wind speed = 5 m/s). The surface
 653 topography is idealized, but similar to that documented by Zuhr et al. (2021, 2023). We

654 find that air flow can be as much as a few cm/s down to 10 cm in the snow, making in-
655 fluence of the near-surface atmosphere on a shallow, near-surface layer of snow possible.
656 On the other hand, laboratory experiments by (Ebner et al., 2017) show that forced ven-
657 tilation of snow almost certainly causes hand-to-hand exchange within the snow, rather
658 than inducing transport of atmospheric water vapor directly down to different depths
659 as was modeled in Town, Warren, et al. (2008). Combining these ideas, enhanced exchange
660 between the ventilated layers during the summer seems plausible, causing a *net* subli-
661 mation isotopic signal in a 10-15 cm layer of near-surface snow during summertime low-
662 to-no accumulation events at EastGRIP. This is not observed in every season in our record,
663 which points toward more complicated processes likely related to snow redistribution and
664 the surface energy budget.

665 The stratigraphy at EastGRIP documented by Zuhr et al. (2021) is a potential source
666 of temporal isotopic variability when redistribution of settled snow occurs. This is con-
667 sidered a dominant source of spatial stratigraphic noise in isotopic signals in low accu-
668 mulation areas such as EastGRIP (e.g., Münch et al., 2017). The heterogenous snow sur-
669 face structures generated during polar winters have been observed to smooth during sub-
670 sequent summers (e.g., Gow, 1965; Albert, 2002). Zuhr et al. (2021) observed a smooth-
671 ing of the rough snow surface throughout the summer season at EastGRIP, with small
672 negative correlation between variance in surface structure and local winds. The impli-
673 cation here is that scoured areas can fill during precipitation with light-to-moderate winds.
674 During low-to-no accumulation periods like those in focus here other filling mechanisms
675 are also important.

676 Smoothing of sastrugi under relatively moderate winds during summer months at
677 the South Pole has been explained by heating of sastrugi flanks while the Sun spirals around
678 the horizon. Frost is deposited on the backs of dunes and sastrugi under extended pe-
679 riods of clear skies and high temperature inversions (Gow, 1965). Filling of scoured ar-
680 eas results afterwards when the fragile surface facets are toppled by winds of mild or mod-
681 erate intensity. We have witnessed this combined mechanism at EastGRIP. We infer that
682 under common conditions at EastGRIP redistributed snow can have a sublimation/deposition
683 signal. Modeling by Casado et al. (2021) indicates this process could decrease $\delta^{18}O$ and
684 increase d . We presume this mechanism results in a net mass deposition at the surface.
685 Important questions remain here:

- 686 • In what proportion does the mass come from the near-surface atmosphere or snow
687 under these conditions?
- 688 • To what extent does this mechanism occur, either in frequency or in mass trans-
689 fer?

690 Looking ahead, a clear-sighted experiment around frost formation would couple snow
691 and near-surface atmosphere temperature and humidity measurements, as well as their
692 gradients, with time-resolved snow density and isotopic measurements to simulate where
693 the frost mass is coming from. It may be that if mass transfer from subsurface layers is
694 not directly detectable, it can be inferred isotopically.

695 Of course, accumulation provides a fundamental contribution to the isotopic sig-
696 nal of snow. In the context of post-depositional processes, a high accumulation rate will
697 advect snow away from the influence of the near-surface atmosphere quickly (e.g., Town,
698 Warren, et al., 2008). In 2018, there is almost 20 cm of accumulation during our obser-
699 vation period, which removes the late Spring/early Summer from the influence of the near-
700 surface summer atmosphere according to our analysis.

701 The observations presented here are complicated enough that a more comprehen-
702 sive approach is necessary to clearly distill the processes at work and their relative im-
703 portance during the polar summer. Such an approach would in cloud amount, isotopic
704 content, and frequency of precipitation and redistributed snow, as well as magnitude and
705 variability of latent heat fluxes. We make recommendations in Section 4.2 to this effect.

706 **4.1.2 Interannual**

707 There does not seem to be clear interannual changes in $\delta^{18}O$ between the mean pro-
708 files presented above. Using the same isotopic-gradient diffusion scenario as in Section 4.1.1
709 we simulate $\Delta\delta^{18}O/\Delta T$ can change at a rate of $0.16\pm 0.03 \text{ } \text{‰}\cdot\text{ } ^\circ\text{C}^{-1}\cdot\text{year}^{-1}$ ($p < 0.05$),
710 effectively the same rate we observe in our data. However, the mean d signal in summer
711 snow experiences an increase of up to $5 \text{ } \text{‰}$ after one year in the snow (Figure 5) due
712 to a shifting and broadening of the Autumn d peak. Although this almost the same mag-
713 nitude of a sublimation-induced decrease in d that *can* happen through a low-accumulation
714 summer season, we believe these processes are not explicitly linked.

715 The shift in d peak can be partially explained by (Johnsen et al., 2000) isotopic-
 716 gradient-driven diffusion. Our simulations of an annual cycle of isotopic-gradient-driven
 717 diffusion on the mean 2019 $\delta^{18}O$ and δD profiles result in a broadening and a downward
 718 (backward in time) shifting of the Autumn d peak (See Appendix, Figure B1). This Au-
 719 tumn peak broadening in d results in a d increase of 2-5 ‰ in the summer snow lay-
 720 ers, similar to our observations. What is also present in the simulations, but missing from
 721 the observations, is an adjacent negative excursion in d in the previous spring snow layer.
 722 The isotopic-gradient diffusion smooths signals, resulting in no net bias. The snow pro-
 723 file observations show a bias induced in d . Sensitivity tests find that applying the dif-
 724 fusion simulations to smoother mean profiles as opposed to individual profiles with sharper
 725 features underestimates the amount of isotopic-gradient diffusion. A more mechanistic
 726 study is necessary here resolve specific processes at work and better understand the smooth-
 727 ing and potential biases.

728 The increase in summer layer d most likely occurs during the following Autumn
 729 when snow temperatures are still relatively high and snow temperature gradients are also
 730 very high (e.g., Town, Waddington, et al., 2008). The summer layers during their first
 731 year in the snow have a $\delta^{18}O$ vs δD slope of 7.87 $\delta D/\delta^{18}O$, which changes to 8.56 ‰·
 732 ‰⁻¹ after one year in the snow (Table A6). This represents dramatic resetting of the
 733 meteoric water line relationship after advection away from the direct influence of the near-
 734 surface atmosphere. We suggest a mechanism of temperature-gradient-driven intersti-
 735 tial vapor diffusion. Even though interstitial air flow will be low as these summer lay-
 736 ers are advected downwards, there are still large synoptically and seasonally driven tem-
 737 perature gradients in the snow down to 50 cm (Town, Waddington, et al., 2008). Rel-
 738 atively high temperature gradients and increasing temperatures also occur during late
 739 Spring. At EastGRIP, a summer snow layer that has been buried for three-quarters of
 740 a year will be almost 30 cm away from the surface. So, we consider Spring a less likely
 741 candidate for timing of d increase as the synoptic and seasonal temperature gradients
 742 rapidly decrease in strength when moving away from the surface snow (Town, Warren,
 743 et al., 2008).

744 These results are fairly independent of the age-depth model because the model for-
 745 mulation first relies on tying together like features in the $\delta^{18}O$ profiles first, then assign-
 746 ing a specific date to each $\delta^{18}O$ feature. Shifts d peaks are then understood as shifts in

747 δD relative to $\delta^{18}O$, as expected due to the different diffusion coefficients (Hellmann &
 748 Harvey, 2020), irrespective of the dates assigned to a given profile depth.

749 4.2 Implications and Future Work

750 We find that d can undergo significant post-depositional change both during a sum-
 751 mer season and over one-to-two years in the firn. Summer precipitation that falls at East-
 752 GRIP with elevated d values can experience a sublimation-induced decrease just after
 753 deposition, and then a subsequent increase likely due to vapor-pressure-gradient induced
 754 post-depositional change deeper in the firn. It seems that d not only has information about
 755 source region and transport history, but also integrates the local near-surface snow his-
 756 tory at sites where meteorologically-induced post-depositional isotopic change in near
 757 surface snow occurs. In these data, mean summer layer d decreases by up to 5 ‰ due
 758 to sublimation prior to being advected away from the direct influence of the near-surface
 759 atmosphere. Prior literature indicates the largest post-depositional change occurs at sites
 760 characterized by a combination of relatively low accumulation, relatively high surface tem-
 761 peratures and vapor pressures, high winds, and high surface relief (Waddington et al.,
 762 2002; Neumann & Waddington, 2004; Town, Warren, et al., 2008). The specific combi-
 763 nation of these factors for a given site requires process-based models of the near-surface
 764 snow to be coupled with IEMs for proper characterization.

765 We show that significant enrichment of $\delta^{18}O$ can happen in the near-surface snow
 766 after deposition during summertime low-to-no accumulation events. This is likely due
 767 to sublimation, consistent with previous observations and modeling for surface snow at
 768 EastGRIP (Wahl et al., 2022). The $\delta^{18}O$ content of snow is often used as a regional tem-
 769 perature proxy, whether local atmospheric temperature or cloud temperature, because
 770 of aforementioned strong spatial and temporal relationships between $\delta^{18}O$ and temper-
 771 ature. However, our results in the context of broader literature base (e.g., Casado et al.,
 772 2021; Wahl et al., 2022) indicate that the $\delta^{18}O$ is probably much better interpreted as
 773 a surface energy budget proxy, or a combined temperature and latent heat flux proxy.

774 A more nuanced interpretation of the $\delta^{18}O$, or δD , proxy is particularly important
 775 to studies like Jones et al. (2023), who interpret summer-only δD changes in West Antarc-
 776 tica as changes in summer temperature due to changes in insolation. Interpreting changes
 777 in δD as both changes in temperature and latent heat flux could help explain why the

778 West Antarctic summer δD pattern is correlated with Milankovitch insolation patterns
779 even though annually coincident winter correlation in δD is not clearly evident. Simi-
780 larly, studies using $\delta^{18}O$ as summer or annual temperature proxies in ice sheet elevation
781 reconstructions may be biased warm due to influence of sublimation on $\delta^{18}O$ (e.g., P. M. Grootes
782 & Stuiver, 1987; Lecavalier et al., 2013; Badgeley et al., 2022), likely yielding a thinner
783 ice sheets than were actually present.

784 Isotope-enabled GCMs (Werner et al., 2011) and cloud physics schemes (e.g., Pe-
785 tit et al., 1991; Ciais & Jouzel, 1994; Dürsch et al., 2019) designed to leverage the d pa-
786 rameter over the polar regions are routinely trained on polar surface snow or deep ice
787 cores. These efforts may be at risk of heuristically incorporating post-depositional pro-
788 cesses into their cloud physics or super saturation schemes. Similarly, a recent definition
789 of d optimized for cold climates used surface snow as ground truth without assessment
790 of the surface snow’s d vulnerability to post-depositional change (Uemura et al., 2012).

791 Changes in near-surface snow due to the influence of the atmosphere or temper-
792 ature gradients in the snow are possible at any time of the year. Our data set can pri-
793 marily tell us about the changes in summer snow layers during summertime and inter-
794 annually. When we extract snow, the timing of accumulation to advect snow away from
795 the surface, and seasonal temperature and humidity are part of our detection bias. We
796 expect most isotopic change to occur during summer and warm periods during shoul-
797 der seasons due to higher vapor pressures and vapor pressure gradients in the atmosphere
798 and near-surface snow. Vapor-pressure-gradient-induced post-depositional change may
799 occur in other seasons soon after deposition, but we are not able to detect this due to
800 extraction timing. For example, we see that the near-surface atmosphere has influence
801 at EastGRIP down to 10-15 cm where the accumulation rate is 40 cm/year (Figures 6-
802 9). In this case, it is possible that snow from a low-accumulation Spring may undergo
803 post-depositional isotopic change during a subsequent Summer.

804 To better interpret $\delta^{18}O$ and d as proxies for climate, we see the need for improved
805 field experimentation to characterize seasonally-dependent post-depositional change. This
806 would manifest as longer sampling periods, possibly annual in duration, over a period
807 of years to document the scope of post-depositional change at a range of sites vulner-
808 able to post-depositional change. Data sets such as these would help our second recom-
809 mendation: further development of streamlined, site-agnostic process-based models that

810 include the impact of the surface energy budget, near-surface snow vapor dynamics, and
811 redistribution processes on the isotopic content of near-surface snow (e.g., Town, War-
812 ren, et al., 2008; Touzeau et al., 2018; Stevens et al., 2020; Kahle et al., 2021; Hughes
813 et al., 2021; Casado et al., 2021; Wahl et al., 2022). This combination will allow for train-
814 ing of model parameters and investigation into compensating impacts of all potential pro-
815 cesses impacting post-depositional isotopic change of near-surface snow. Coupling of the
816 near-surface models with existing meteorological and climate IEMs will have the poten-
817 tial to refine all reconstructions of past climate based on water isotopic content of po-
818 lar ice cores.

819 4.3 Conclusions

820 Water isotopes in polar snow have historically been used to infer information about
821 past climates of polar ice sheets, as well as the integrated history of polar precipitation.
822 These inferences rely on a continuous physical understanding of the water’s history, from
823 source to extraction. A weak link in this understanding exists in the near-surface polar
824 snow where dynamic snow metamorphism occurs under the influence of local meteorol-
825 ogy and climate. This data set provides successive looks at the same snow layers, allow-
826 ing us to document how the near-surface snow ages isotopically on two timescales, dur-
827 ing summer and interannually. We use surface and near-surface snow extracted from the
828 EastGRIP site in NE Greenland during summer months of 2017-2019 to help address
829 this gap in understanding, as such our conclusions about the summer layers are strongest.

830 Near-surface snow collected during the same summer season shows isotopic signa-
831 tures of sublimation down to 10-15 cm as the snow ages during low-to-no accumulation
832 events. This depth is consistent with the depths of wind-pumping likely present at East-
833 GRIP, indicating the potential influence of the near-surface atmosphere. The combined
834 $\delta^{18}O$ and d sublimation signature is inconsistent from season-to-season, pointing to the
835 need for more process-based understanding. The mean summer surface snow d is always
836 greater than the mean d from snow profiles extracted later in the season, indicating sub-
837 limation through the summer season. It is possible that similar changes are occurring
838 shortly after deposition in other seasons at relatively warm or low accumulation sites,
839 particularly during early Autumn and late Spring.

840 We see significant increases in d of up to 5 ‰ in the summer layers after one-to-
 841 two years of aging in the firn. We see decreases in d in other seasonal layers, but these
 842 decreases do not rise to the level of $p < 0.05$. The increases we observe in summer layer
 843 d are coincidentally almost the same the magnitude as the decrease in d observed dur-
 844 ing some summer seasons immediately after deposition. No coincident interannual change
 845 in $\delta^{18}O$ is observable in our data. There is a significant decrease in seasonal $\Delta\delta^{18}O/\Delta T$
 846 over our study period, but more work is necessary to determine the pattern and rate of
 847 this change.

848 Mechanisms for the changes during summer months include a combination of isotopic-
 849 gradient-driven diffusion and wind-enhanced net sublimation from the near-surface snow.
 850 We postulate that some summer wind-driven redistribution events can have distinct sub-
 851 limation/deposition signatures after surface faceting events. Interannually, isotopic-gradient
 852 diffusion can explain the changes in seasonal isotope-temperature sensitivity. It also ex-
 853 plains some but not all of the Δd pattern we observe. We suspect seasonally- and synoptically-
 854 induced vapor-pressure gradients in the near-surface snow to be an important metamor-
 855 phic process during Spring, Summer, and Autumn months. They ought to be less im-
 856 portant during Winter months due to the low interstitial vapor pressures.

857 Our observations are relevant for the interpretation of water isotopes as proxies for
 858 past climates in polar regions. Intermittent summer enrichment of surface and near-surface
 859 $\delta^{18}O$ indicates that this proxy should likely be interpreted as an integrated local cloud
 860 or surface temperature *and* near-surface latent heat budget proxy. Similarly, the sum-
 861 mer and interannual evolution of d shown here indicates that d is not only a proxy for
 862 water source region conditions and transport history, but also integrates local meteorol-
 863 ogy and climate information in the months and years after deposition - at least in sum-
 864 mer snow layers.

865 Our results are complicated by the extractive nature of the observations, where spa-
 866 tial variability is at risk of being interpreted as temporal variability. Our strategic spatially-
 867 distributed sampling program coupled with the depth corrections and an age-depth model
 868 puts most of the stratigraphic noise in our error bars, but of course not all.

869 Our results are specific to the present day climate at EastGRIP, a relatively warm
 870 but low accumulation site on the Greenland Ice Sheet. These results are consistent with
 871 prior work exploring and documenting post-depositional processes (e.g. Waddington et

872 al., 2002; Neumann et al., 2005; Town, Warren, et al., 2008; Steen-Larsen et al., 2014;
 873 Casado et al., 2021; Hughes et al., 2021; Wahl et al., 2021), and demonstrate that more
 874 general revisions to interpretations of water isotope proxies in polar snow are needed.
 875 Questions remain about potential changes in other seasons, as well as the mechanisms
 876 at work and their relative importance. We also still lack generalized tools for assessing
 877 near-surface post-depositional modification of water isotope proxies at ice core sites, which
 878 are critical for interpretation of water-isotope-based climate records.

879 We recommend further field work documenting the annual evolution of the near-
 880 surface snow with successive snow profiles overlapping in their depth, but also assess-
 881 ing spatial variability. These data, an extension of those presented here, will act as a train-
 882 ing ground for the development of isotope-enabled, process-based models of the near-surface
 883 snow. Driving, or coupling, the near-surface snow models with meteorological IEMs will
 884 greatly advance site-agnostic means for interpretation of past climates using polar snow.

885 **Appendix A Tables of snow profile statistics**

886 We provide tables of statistics for the snow profiles and their changes presented in
 887 Figures 3(c,d) and 4(c,d) composited by season or year.

888 **Appendix B Supporting simulations**

889 **B1 Isotope-gradient-driven diffusion simulations**

890 We use the Johnsen et al. (2000) isotopic-gradient-driven diffusion model to assess
 891 the potential impact of this mechanism to explain the pattern and magnitude of the changes
 892 we observe in the near-surface snow at EastGRIP. The model is run on the mean $\delta^{18}O$
 893 and δD profiles from the 2019 field season using the following scenario that roughly ap-
 894 proximates the seasonal cycle at EastGRIP: Summer is 60 days with snow at $-11^{\circ}C$, Au-
 895 tumn is 60 days with snow at $-28.5^{\circ}C$, Winter is 180 days with snow at $-40^{\circ}C$, Spring
 896 is 60 days with snow at $-28.5^{\circ}C$. This scenario is realistic, but will overestimate the amount
 897 of diffusion due to the long warm summer used.

898 The magnitude of the annual $\delta^{18}O$ and d changes due to this process are on the
 899 order of what we observe as annual changes in the snow profiles. The largest changes in
 900 the simulation occur during the warmest months and around the largest isotopic gra-
 901 dents. There was not a significant change in $\delta^{18}O$ observed beyond the uncertainty in

902 the snow profile averages, so we are not able to differentiate interannual $\Delta\delta^{18}O$ due to
903 isotopic gradient diffusion from stratigraphic noise.

904 However, the interannual Δd in the summer layers was significant. Figure B1 shows
905 a simulated interannual Δd due only to Johnsen et al. (2000) diffusion, using the 2019
906 mean snow profiles as a starting point. A large positive bias in d , up to 5 ‰, can be
907 seen in the summer layers after one year of isotopic-gradient-driven diffusion. This is sim-
908 ilar to what we observe in the snow profiles (e.g. Figures 4(d) and 5(b)). However, the
909 large positive excursion is preceded in time with a similarly large negative change in d .
910 The Johnsen et al. (2000) model smooths isotopic signals, and shifts the d peaks down-
911 ward, towards 'earlier' times. However, this behavior is not found in the observations.

912 Isotopic gradient diffusion is very likely at work in the near-surface snow during
913 relatively warm months, particularly after the snow has been advected away from the
914 influence of near-surface atmospheric winds (i.e. wind-pumping effects).

915 **Open Research Section**

916 All data used in this study are available for use and can be found at www.pangaea.de.
917 Specific references follow. The bamboo snow stake data as described in Section 2.1 can
918 be found at (Steen-Larsen, 2020a, 2020b; Harris Stuart et al., 2023). The snow surface
919 isotope data as described in Section 2.2 can be found at (Hörhold et al., 2023; Hörhold,
920 Behrens, Hoffmann, et al., 2022; Hörhold et al., 2022; Hörhold, Behrens, Wahl, et al.,
921 2022). The raw measurements for the snow profile data as described in Section 2.3.1 can
922 be found at (Behrens et al., 2023). The snow profile data with depth correction and age-
923 depth model as described in Section 2.3.1, Section 2.4.1, and Section 2.4.2 be found at
924 (Town et al., 2023).

925 **Acknowledgments**

926 This project has received funding from the European Research Council (ERC) un-
927 der the European Union's Horizon 2020 research and innovation program: Starting Grant-
928 SNOWISO (grant agreement 759526).

929 EastGRIP is directed and organized by the Centre for Ice and Climate at the Niels
930 Bohr Institute, University of Copenhagen. It is supported by funding agencies and insti-
931 tutions in Denmark (A. P. Møller Foundation, University of Copenhagen), USA (US Na-

932 tional Science Foundation, Office of Polar Programs), Germany (Alfred Wegener Insti-
 933 tute, Helmholtz Centre for Polar and Marine Research), Japan (National Institute of Po-
 934 lar Research and Arctic Challenge for Sustainability), Norway (University of Bergen and
 935 Bergen Research Foundation), Switzerland (Swiss National Science Foundation), France
 936 (French Polar Institute Paul-Émile Victor, Institute for Geosciences and Environmen-
 937 tal research), and China (Chinese Academy of Sciences and Beijing Normal University).

938 Many talented workers helped in the collection and measurement of the snow. Basile
 939 de Fleurian, Johannes Frietag, Abby Hughes, Emma Kahle, Martin Madsen, Hannah Meyer,
 940 Silje Smith-Johnsen, Alexandra Touzeau, Diana Vladimirova, and Tobias Zolles assisted
 941 in the field with snow collection and processing. Þorsteinn Jónsson and Rósa Ólafsdót-
 942 tir assisted in the isotopic measurement of snow.

943 Author contributions are as follows: MST and HCSL designed the study. HCSL,
 944 AKF, SW, MB, MH, and AZ obtained the observational dataset. MB, MH, and AS an-
 945 alyzed the snow samples. MST and MB curated and processed the snow profile data set.
 946 MST performed the formal analysis and wrote the manuscript. HCSL, TJ, and SW con-
 947 tributed to the interpretation of the analyses. Reviews and edits were made by all co-
 948 authors. HCSL designed and acquired funding for this study and administrated the SNOW-
 949 ISO project.

950 References

- 951 Albert, M. R. (2002). Effects of snow and firm ventilation on sublimation rates. *An-*
 952 *nals of Glaciology*, *35*, 52-56. doi: 10.3189/172756402781817194
- 953 Badgeley, J. A., Steig, E. J., & Dütsch, M. (2022, 12). Uncertainty in reconstructing
 954 paleo-elevation of the antarctic ice sheet from temperature-sensitive ice core
 955 records. *Geophysical Research Letters*, *49*. doi: 10.1029/2022GL100334
- 956 Behrens, M., Town, M. H. M. S., , & Steen-Larsen, H. C. (2023). *Snow profiles of*
 957 *stable water isotopes at the eastgrip deep drilling site, summer seasons 2016*
 958 *- 2019* [data set]. PANGAEA. Retrieved from PANGAEAdatasubmission:
 959 PDI-33944
- 960 Blossey, P. N., Kuang, Z., & Romps, D. M. (2010). Isotopic composition of water
 961 in the tropical tropopause layer in cloud-resolving simulations of an idealized
 962 tropical circulation. *Journal of Geophysical Research Atmospheres*, *115*. doi:

- 963 10.1029/2010JD014554
- 964 Bolzan, J. F., & Pohjola, V. A. (2000, 9). Reconstruction of the undiffused seasonal
965 oxygen isotope signal in central greenland ice cores. *Journal of Geophysical Re-*
966 *search: Oceans*, *105*, 22095-22106. doi: 10.1029/2000jc000258
- 967 Buizert, C., Fudge, T. J., Roberts, W. H. G., Steig, E. J., Sherriff-Tadano, S., Ritz,
968 C., . . . Schwander, J. (2021). *Antarctic surface temperature and elevation*
969 *during the last glacial maximum* (Vol. 372).
- 970 Casado, M., Landais, A., Picard, G., Arnaud, L., Dreossi, G., Stenni, B., & Prié,
971 F. (2021, 9). Water isotopic signature of surface snow metamorphism in
972 antarctica. *Geophysical Research Letters*, *48*. doi: 10.1029/2021GL093382
- 973 Casado, M., Landais, A., Picard, G., Münch, T., Laepple, T., Stenni, B., . . . Jouzel,
974 J. (2018, 5). Archival processes of the water stable isotope signal in east
975 antarctic ice cores. *Cryosphere*, *12*, 1745-1766. doi: 10.5194/tc-12-1745-2018
- 976 Charles, C. D., Rind, D., Jouzel, J., Koster, R. D., & Fairbanks, R. G. (1994).
977 *Glacial-interglacial changes in moisture sources for greenland: Influences on*
978 *the ice core record of climate* (Vol. 263).
- 979 Ciais, P., & Jouzel, J. (1994). Deuterium and oxygen 18 in precipitation: Isotopic
980 model, including mixed cloud processes. *Journal of Geophysical Research*, *99*,
981 16793-16803. doi: 10.1029/94JD00412
- 982 Colbeck, S. C. (1983). Theory of metamorphism of dry snow. *Journal of Geophysical*
983 *Research*, *88*, 5475-5482. doi: 10.1029/JC088iC09p05475
- 984 Colbeck, S. C. (1989). Air movement in snow due to windpumping. *Journal of*
985 *Glaciology*, *35*, 209-213. doi: 10.3189/s0022143000004524
- 986 Colbeck, S. C. (1997). Model of wind pumping for layered snow. *Journal of Glaciol-*
987 *ogy*, *43*, 60-65. doi: 10.3189/s002214300000280x
- 988 Craig, H. (1961). Isotopic variations in meteoric waters. *Science*, *133*, 1702-1703.
989 doi: 10.1126/science.133.3465.1702
- 990 Craig, H., & Gordon, L. I. (1965). Deuterium and oxygen 18 variations in the ocean
991 and the marine atmosphere. In E. Tongiorgi (Ed.), *Stable isotopes in oceano-*
992 *graphic studies and paleotemperatures* (p. 9–130).
- 993 Cuffey, K. M., Clow, G. D., Alley, R. B., Stuiver, M., Waddington, E. D., & Saltus,
994 R. W. (1995). Large arctic temperature change at the wisconsin-holocene
995 glacial transition. *Science*, *270*, 455-458.

- 996 Cuffey, K. M., Clow, G. D., Steig, E. J., Buizert, C., Fudge, T. J., Koutnik, M., ...
 997 Severinghaus, J. P. (2016, 12). Deglacial temperature history of west antarctica.
 998 *Proceedings of the National Academy of Sciences of the United States of*
 999 *America*, *113*, 14249-14254. doi: 10.1073/pnas.1609132113
- 1000 Dahl-Jensen, D., Albert, M. R., Aldahan, A., Azuma, N., Balslev-Clausen, D.,
 1001 Baumgartner, M., ... Zheng, J. (2013, 1). Eemian interglacial recon-
 1002 structed from a greenland folded ice core. *Nature*, *493*, 489-494. doi:
 1003 10.1038/nature11789
- 1004 Dansgaard, W. (1964, 11). Stable isotopes in precipitation. *Tellus*, *16*, 436-468. doi:
 1005 10.1111/j.2153-3490.1964.tb00181.x
- 1006 Dee, S., Emile-Geay, J., Evans, M. N., Allam, A., Steig, E. J., & Thompson, D. M.
 1007 (2015, 9). Prysm: An open-source framework for proxy system modeling, with
 1008 applications to oxygen-isotope systems. *Journal of Advances in Modeling Earth*
 1009 *Systems*, *7*, 1220-1247. doi: 10.1002/2015MS000447
- 1010 Dütsch, M., Blossey, P. N., Steig, E. J., & Nusbaumer, J. M. (2019, 11). Nonequi-
 1011 librium fractionation during ice cloud formation in icam5: Evaluating the
 1012 common parameterization of supersaturation as a linear function of temper-
 1013 ature. *Journal of Advances in Modeling Earth Systems*, *11*, 3777-3793. doi:
 1014 10.1029/2019MS001764
- 1015 Ebner, P. P., Steen-Larsen, H. C., Stenni, B., Schneebeli, M., & Steinfeld, A. (2017,
 1016 7). Experimental observation of transient 18o interaction between snow and
 1017 advective airflow under various temperature gradient conditions. *Cryosphere*,
 1018 *11*, 1733-1743. doi: 10.5194/tc-11-1733-2017
- 1019 Epstein, S., Sharp, R. P., & Gow, A. J. (1965). Six-year record of oxygen and hydro-
 1020 gen isotope variations in south pole firn. *JOURNAL OF GEOPHYSICAL RE-*
 1021 *SEARCH*, *20*.
- 1022 Fausto, R. S., As, D. V., Mankoff, K. D., Vandecrux, B., Citterio, M., Ahlström,
 1023 A. P., ... Box, J. E. (2021, 8). Programme for monitoring of the greenland ice
 1024 sheet (promice) automatic weather station data. *Earth System Science Data*,
 1025 *13*, 3819-3845. doi: 10.5194/essd-13-3819-2021
- 1026 Filhol, S., & Sturm, M. (2015, 9). Snow bedforms: A review, new data, and a forma-
 1027 tion model. *Journal of Geophysical Research: Earth Surface*, *120*, 1645-1669.
 1028 doi: 10.1002/2015JF003529

- 1029 Fisher, D. A., Reeh, N., & Clausen, H. (1985). Stratigraphic noise in time se-
 1030 ries derived from ice cores. *Annals of Glaciology*, *7*, 76-83. doi: 10.3189/
 1031 s0260305500005942
- 1032 Fujita, K., & Abe, O. (2006, 9). Stable isotopes in daily precipitation at dome
 1033 fuji, east antarctica. *Geophysical Research Letters*, *33*. doi: 10.1029/
 1034 2006GL026936
- 1035 Gkinis, V., Simonsen, S. B., Buchardt, S. L., White, J. W., & Vinther, B. M. (2014,
 1036 11). Water isotope diffusion rates from the northgrip ice core for the last
 1037 16,000 years - glaciological and paleoclimatic implications. *Earth and Plane-
 1038 tary Science Letters*, *405*, 132-141. doi: 10.1016/j.epsl.2014.08.022
- 1039 Gonfiantini, R. (1978). Standards for stable isotope measurements in natural com-
 1040 pounds. *Nature*, *271*, 534-536. doi: <http://dx.doi.org/10.1038/271534a0>
- 1041 Gow, A. J. (1965). On the accumulation and seasonal stratification of snow
 1042 at the south pole. *Journal of Glaciology*, *5*, 467-477. doi: 10.3189/
 1043 s002214300001844x
- 1044 Grootes, P., Stuiver, M., White, J. W. C., Johnsen, S., & Jouzel, J. (1993). Compar-
 1045 ison of oxygen isotope records from the gisp2 and grip greenland ice cores. *Na-
 1046 ture*, *366*, 552-554.
- 1047 Grootes, P. M., & Stuiver, M. (1987). *Ice sheet elevation changes from isotope pro-
 1048 files* (Vol. 170). IAHS Publ.
- 1049 Guillevic, M., Bazin, L., Landais, A., Kindler, P., Orsi, A., Masson-Delmotte, V., ...
 1050 Vinther, B. M. (2013). Spatial gradients of temperature, accumulation and
 1051 18o- ice in greenland over a series of dansgaard-oeschger events. *Climate of the
 1052 Past*, *9*, 1029-1051. doi: 10.5194/cp-9-1029-2013
- 1053 Harris Stuart, R., Faber, A.-K., Wahl, S., Hörhold, M., Kipfstuhl, S., Vasskog, K.,
 1054 ... Steen-Larsen, H. C. (2023). Exploring the role of snow metamorphism
 1055 on the isotopic composition of the surface snow at eastgrip. *The Cryosphere*,
 1056 *17*(3), 1185-1204. doi: 10.5194/tc-17-1185-2023
- 1057 Hellmann, R., & Harvey, A. H. (2020, 9). First-principles diffusivity ratios for kinetic
 1058 isotope fractionation of water in air. *Geophysical Research Letters*, *47*. doi: 10
 1059 .1029/2020GL089999
- 1060 Hörhold, M., Behrens, M., Hoffmann, A., Faber, A.-K., Kahle, E., Freitag, J., ...
 1061 Steen-Larsen, H. C. (2022). *Snow stable water isotopes of a surface transect*

- 1062 *at the eastgrip deep drilling site, summer season 2017* [data set]. PANGAEA.
 1063 Retrieved from PANGAEAdatasubmission:PDI-33947
- 1064 Hörhold, M., Behrens, M., Vladimirova, D., Madsen, M., & Steen-Larsen, H. C.
 1065 (2023). *Snow stable water isotopes of a surface transect at the eastgrip deep*
 1066 *drilling site, summer season 2016* [data set]. PANGAEA. Retrieved from
 1067 PANGAEAdatasubmission:PDI-33945
- 1068 Hörhold, M., Behrens, M., Wahl, S., Faber, A.-K., Zuhr, A., Meyer, H., & Steen-
 1069 Larsen, H. C. (2022). *Snow stable water isotopes of a surface transect at*
 1070 *the EastGRIP deep drilling site, summer season 2019* [data set]. PAN-
 1071 GAEA. Retrieved from <https://doi.org/10.1594/PANGAEA.945563> doi:
 1072 10.1594/PANGAEA.945563
- 1073 Hörhold, M., Behrens, M., Wahl, S., Faber, A.-K., Zuhr, A., Zolles, T., & Steen-
 1074 Larsen, H. C. (2022). *Snow stable water isotopes of a surface transect at*
 1075 *the EastGRIP deep drilling site, summer season 2018* [data set]. PAN-
 1076 GAEA. Retrieved from <https://doi.org/10.1594/PANGAEA.945544> doi:
 1077 10.1594/PANGAEA.945544
- 1078 Hu, J., Yan, Y., Yeung, L. Y., & Dee, S. G. (2022, 6). Sublimation origin of negative
 1079 deuterium excess observed in snow and ice samples from mcmurdo dry valleys
 1080 and allan hills blue ice areas, east antarctica. *Journal of Geophysical Research:*
 1081 *Atmospheres*, 127. Retrieved from [https://onlinelibrary.wiley.com/doi/](https://onlinelibrary.wiley.com/doi/10.1029/2021JD035950)
 1082 [10.1029/2021JD035950](https://onlinelibrary.wiley.com/doi/10.1029/2021JD035950) doi: 10.1029/2021JD035950
- 1083 Hudson, S. R., & Brandt, R. E. (2005). A look at the surface-based temperature in-
 1084 version on the antarctic plateau. *Journal of Climate*.
- 1085 Hughes, A. G., Wahl, S., Jones, T. R., Zuhr, A., Hörhold, M., White, J. W., &
 1086 Steen-Larsen, H. C. (2021, 10). The role of sublimation as a driver of climate
 1087 signals in the water isotope content of surface snow: Laboratory and field ex-
 1088 perimental results. *Cryosphere*, 15, 4949-4974. doi: 10.5194/tc-15-4949-2021
- 1089 Johnsen, S. (1977). Stable isotope homogenization of polar firn and ice. *In: Proc.*
 1090 *Symp. on Isotopes and Impurities in Snow and Ice, I.U.G.G. XVI, General*
 1091 *Assembly, 1975*, 210–219.
- 1092 Johnsen, S., Clausen, H. B., Cuffey, K. M., Hoffmann, G., Schwander, J., & Creyts,
 1093 T. (2000). *Diffusion of stable isotopes in polar firn and ice: the isotope effect*
 1094 *in firn diffusion*. Hokkaido University Press.

- 1095 Johnsen, S., Dahl-Jensen, D., Gundestrup, N., Steffensen, J. P., Clausen, H. B.,
 1096 Miller, H., . . . White, J. (2001). Oxygen isotope and palaeotemperature
 1097 records from six greenland ice-core stations: Camp century, dye-3, grip, gisp2,
 1098 renland and northgrip. *Journal of Quaternary Science*, *16*, 299-307. doi:
 1099 10.1002/jqs.622
- 1100 Johnsen, S., & White, J. W. C. (1989). The origin of arctic precipitation under
 1101 present and glacial conditions. *Tellus*, *418*, 452-468.
- 1102 Jones, T. R., Cuffey, K. M., Roberts, W. H., Markle, B. R., Steig, E. J., Stevens,
 1103 C. M., . . . White, J. W. (2023, 1). Seasonal temperatures in west antarctica
 1104 during the holocene. *Nature*, *613*, 292-297. doi: 10.1038/s41586-022-05411-8
- 1105 Jones, T. R., Cuffey, K. M., White, J. W., Steig, E. J., Buizert, C., Markle, B. R.,
 1106 . . . Sigl, M. (2017, 1). Water isotope diffusion in the wais divide ice core
 1107 during the holocene and last glacial. *Journal of Geophysical Research: Earth
 1108 Surface*, *122*, 290-309. doi: 10.1002/2016JF003938
- 1109 Jones, T. R., Roberts, W. H., Steig, E. J., Cuffey, K. M., Markle, B. R., &
 1110 White, J. W. (2018, 2). Southern hemisphere climate variability forced
 1111 by northern hemisphere ice-sheet topography. *Nature*, *554*, 351-355. doi:
 1112 10.1038/nature24669
- 1113 Jouzel, J., Alley, R. B., Cuffey, K. M., Dansgaard, W., Grootes, P., Hoffmann, G.,
 1114 . . . White, J. (1997, 11). Validity of the temperature reconstruction from
 1115 water isotopes in ice cores. *Journal of Geophysical Research: Oceans*, *102*,
 1116 26471-26487. doi: 10.1029/97JC01283
- 1117 Jouzel, J., & Merlivat, L. (1984). *Deuterium and oxygen 18 in precipitation' model-
 1118 ing of the isotopic effects during snow formation* (Vol. 89).
- 1119 Jouzel, J., Vimeux, F., Caillon, N., Delaygue, G., Hoffmann, G., Masson-Delmotte,
 1120 V., & Parrenin, F. (2003, 6). Magnitude of isotope/temperature scaling for
 1121 interpretation of central antarctic ice cores. *Journal of Geophysical Research
 1122 Atmospheres*, *108*. doi: 10.1029/2002jd002677
- 1123 Kahle, E. C., Steig, E. J., Jones, T. R., Fudge, T. J., Koutnik, M. R., Morris, V. A.,
 1124 . . . White, J. W. (2021, 7). Reconstruction of temperature, accumulation
 1125 rate, and layer thinning from an ice core at south pole, using a statistical
 1126 inverse method. *Journal of Geophysical Research: Atmospheres*, *126*. doi:
 1127 10.1029/2020JD033300

- 1128 Kavanaugh, J. L., & Cuffey, K. M. (2003). Space and time variation of $\delta^{18}O$ and δD
 1129 in antarctic precipitation revisited. *Global Biogeochemical Cycles*, *17*. doi: 10
 1130 .1029/2002GB001910
- 1131 King, J. C., & Turner, J. (2009). *Antarctic meteorology and climatology*. Cambridge
 1132 University Press. doi: 10.1017/cbo9780511524967.006
- 1133 Kochanski, K., Anderson, R. S., & Tucker, G. E. (2018, 7). Statistical classification
 1134 of self-organized snow surfaces. *Geophysical Research Letters*, *45*, 6532-6541.
 1135 doi: 10.1029/2018GL077616
- 1136 Komuro, Y., Nakazawa, F., Hirabayashi, M., Goto-Azuma, K., Nagatsuka, N.,
 1137 Shigezawa, W., ... Dahl-Jensen, D. (2021, 3). Temporal and spatial vari-
 1138 abilities in surface mass balance at the egrip site, greenland from 2009 to 2017.
 1139 *Polar Science*, *27*. doi: 10.1016/j.polar.2020.100568
- 1140 Kopec, B. G., Feng, X., Osterberg, E. C., & Posmentier, E. S. (2022, 10). Cli-
 1141 matological significance of $\delta^{18}O$ line slopes from precipitation, snow pits, and
 1142 ice cores at summit, greenland. *Journal of Geophysical Research: Atmo-*
 1143 *spheres*. Retrieved from [https://onlinelibrary.wiley.com/doi/10.1029/](https://onlinelibrary.wiley.com/doi/10.1029/2022JD037037)
 1144 [2022JD037037](https://onlinelibrary.wiley.com/doi/10.1029/2022JD037037) doi: 10.1029/2022JD037037
- 1145 Laepple, T., Münch, T., Casado, M., Hoerhold, M., Landais, A., & Kipfstuhl, S.
 1146 (2018, 1). On the similarity and apparent cycles of isotopic variations in east
 1147 antarctic snow pits. *Cryosphere*, *12*, 169-187. doi: 10.5194/tc-12-169-2018
- 1148 Lecavalier, B. S., Milne, G. A., Vinther, B. M., Fisher, D. A., Dyke, A. S., & Simp-
 1149 son, M. J. (2013, 3). Revised estimates of greenland ice sheet thinning histo-
 1150 ries based on ice-core records. *Quaternary Science Reviews*, *63*, 73-82. doi:
 1151 10.1016/j.quascirev.2012.11.030
- 1152 Lorius, C., Jouzel, J., Raynaud, D., Hansen, J., & Treut, H. L. (1990). *The ice-core*
 1153 *record: climate sensitivity and future greenhouse warming*.
- 1154 Madsen, M. V., Steen-Larsen, H. C., Hörhold, M., Box, J., Berben, S. M., Capron,
 1155 E., ... Dahl-Jensen, D. (2019, 3). Evidence of isotopic fractionation dur-
 1156 ing vapor exchange between the atmosphere and the snow surface in green-
 1157 land. *Journal of Geophysical Research: Atmospheres*, *124*, 2932-2945. doi:
 1158 10.1029/2018JD029619
- 1159 Magnusson, B., Näykki, T., Hovind, H., Krysell, M., & Sahlin, E. (2017). *Handbook*
 1160 *for calculation of measurement uncertainty in environmental laboratories* (Vol.

- 1161 Nordtest Report TR 537 (ed. 4).
- 1162 Mahrt, L. (2014, 1). Stably stratified atmospheric boundary layers. *Annual Review*
 1163 *of Fluid Mechanics*, *46*, 23-45. doi: 10.1146/annurev-fluid-010313-141354
- 1164 Masson-Delmotte, V., Steen-Larsen, H. C., Ortega, P., Swingedouw, D., Popp, T.,
 1165 Vinther, B. M., ... White, J. W. (2015, 8). Recent changes in north-west
 1166 greenland climate documented by neem shallow ice core data and simulations,
 1167 and implications for past-temperature reconstructions. *Cryosphere*, *9*, 1481-
 1168 1504. doi: 10.5194/tc-9-1481-2015
- 1169 Mayewski, P. A., Meeker, L. D., Whitlow, S., Twickler, M. S., Morrison, M. C.,
 1170 Bloomfield, P., ... Wumkes, W. (1994). Changes in atmospheric circula-
 1171 tion and ocean ice cover over the north atlantic during the last 41,000 years.
 1172 *Science*, *263*, 1747-1751. doi: 10.1126/science.263.5154.1747
- 1173 Merlivat, L., & Jouzel, J. (1979). Global climatic interpretation of the deuterium-
 1174 oxygen 16 relationship for precipitation. *Journal of Geophysical Research*, *84*,
 1175 5029-5033. doi: 10.1029/JC084iC08p05029
- 1176 Mojtabavi, S., Wilhelms, F., Cook, E., Davies, S. M., Sinnl, G., Jensen, M. S., ...
 1177 Rasmussen, S. O. (2020, 11). A first chronology for the east greenland ice-core
 1178 project (egrip) over the holocene and last glacial termination. *Climate of the*
 1179 *Past*, *16*, 2359-2380. doi: 10.5194/cp-16-2359-2020
- 1180 Münch, T., Kipfstuhl, S., Freitag, J., Meyer, H., & Laepple, T. (2016, 7). Regional
 1181 climate signal vs. local noise: A two-dimensional view of water isotopes in
 1182 antarctic firn at kohnen station, dronning maud land. *Climate of the Past*, *12*,
 1183 1565-1581. doi: 10.5194/cp-12-1565-2016
- 1184 Münch, T., Kipfstuhl, S., Freitag, J., Meyer, H., & Laepple, T. (2017, 9). Con-
 1185 straints on post-depositional isotope modifications in east antarctic firn from
 1186 analysing temporal changes of isotope profiles. *Cryosphere*, *11*, 2175-2188. doi:
 1187 10.5194/tc-11-2175-2017
- 1188 Nakazawa, F., Nagatsuka, N., Hirabayashi, M., Goto-Azuma, K., Steffensen, J. P.,
 1189 & Dahl-Jensen, D. (2021, 3). Variation in recent annual snow deposition and
 1190 seasonality of snow chemistry at the east greenland ice core project (egrip)
 1191 camp, greenland. *Polar Science*, *27*. doi: 10.1016/j.polar.2020.100597
- 1192 Neumann, T. A., & Waddington, E. D. (2004). Effects of firn ventilation on
 1193 isotopic exchange. *Journal of Glaciology*, *50*, 183-192. doi: 10.3189/

- 1194 172756504781830150
- 1195 Neumann, T. A., Waddington, E. D., Steig, E. J., & Grootes, P. M. (2005). Non-
 1196 climate influences on stable isotopes at Taylor Mouth, Antarctica. *Journal of*
 1197 *Glaciology*, *51*, 248-258. doi: 10.3189/172756505781829331
- 1198 Petit, J. R., Jouzel, J., Raynaud, D., Barkov, N. I., Barnola, J.-M., Basile, I., ...
 1199 Stievenard, M. (1999). Climate and atmospheric history of the past 420,000
 1200 years from the Vostok ice core, Antarctica: The recent completion of drilling at
 1201 Vostok station in East Antarctica. *Nature*, *399*, 429-436.
- 1202 Petit, J. R., White, J. W., Young, N. W., Jouzel, J., & Korotkevich, Y. S. (1991).
 1203 Deuterium excess in recent Antarctic snow. *Journal of Geophysical Research*,
 1204 *96*, 5113-5122. doi: 10.1029/90JD02232
- 1205 Putnins, P. (1970). The Climate of Greenland. In O. S. (Ed.), *World survey of clima-*
 1206 *tology, vol 14* (p. 3-128). Barking, Essex, England: Elsevier Publishing Com-
 1207 pany LTD.
- 1208 Ritter, F., Steen-Larsen, H. C., Werner, M., Masson-Delmotte, V., Orsi, A., Behrens,
 1209 M., ... Kipfstuhl, S. (2016, 7). Isotopic exchange on the diurnal scale between
 1210 near-surface snow and lower atmospheric water vapor at Kohnen station, East
 1211 Antarctica. *Cryosphere*, *10*, 1647-1663. doi: 10.5194/tc-10-1647-2016
- 1212 Rohling, E. J., Sluijs, A., Dijkstra, H. A., Köhler, P., Wal, R. S. V. D., Heydt,
 1213 A. S. V. D., ... Zeebe, R. E. (2012, 11). Making sense of palaeoclimate
 1214 sensitivity. *Nature*, *491*, 683-691. doi: 10.1038/nature11574
- 1215 Schaller, C. F., Freitag, J., Kipfstuhl, S., Laepple, T., Steen-Larsen, H. C., & Eisen,
 1216 O. (2016, 9). A representative density profile of the North Greenland snowpack.
 1217 *Cryosphere*, *10*, 1991-2002. doi: 10.5194/tc-10-1991-2016
- 1218 Shuman, C. A., Alley, R. B., Anandakrishnan, S., White, J. W. C., Grootes, P. M.,
 1219 & Stearns, C. R. (1995). Temperature and accumulation at the Greenland
 1220 Summit: Comparison of high-resolution isotope profiles and satellite passive
 1221 microwave brightness temperature trends. *JOURNAL OF GEOPHYSICAL*
 1222 *RESEARCH*, *100*.
- 1223 Steen-Larsen, H. C. (2020a). *Snow surface accumulation measured using Bam-*
 1224 *boo stake measurements, EastGRIP camp Greenland, May 2016* [data set]. PAN-
 1225 GAEA. Retrieved from <https://doi.org/10.1594/PANGAEA.921855> doi: 10
 1226 .1594/PANGAEA.921855

- 1227 Steen-Larsen, H. C. (2020b). *Snow surface accumulation measured using SSA*
 1228 *stake measurements, EastGRIP camp Greenland, May 2018* [data set]. PAN-
 1229 GAEA. Retrieved from <https://doi.org/10.1594/PANGAEA.921853> doi:
 1230 10.1594/PANGAEA.921853
- 1231 Steen-Larsen, H. C., Masson-Delmotte, V., Hirabayashi, M., Winkler, R., Satow, K.,
 1232 Prié, F., ... Sveinbjörnsdóttir, A. E. (2014, 2). What controls the isotopic
 1233 composition of greenland surface snow? *Climate of the Past*, *10*, 377-392. doi:
 1234 10.5194/cp-10-377-2014
- 1235 Steen-Larsen, H. C., Masson-Delmotte, V., Sjolte, J., Johnsen, S. J., Vinther, B. M.,
 1236 Bréon, F. M., ... White, J. (2011). Understanding the climatic signal in the
 1237 water stable isotope records from the neem shallow firn/ice cores in north-
 1238 west greenland. *Journal of Geophysical Research Atmospheres*, *116*. doi:
 1239 10.1029/2010JD014311
- 1240 Steffensen, J. P. (1985). Microparticles in snow from the south greenland ice sheet.
 1241 *Tellus B*, *37 B*, 286-295. doi: 10.1111/j.1600-0889.1985.tb00076.x
- 1242 Steffensen, J. P., Andersen, K. K., Bigler, M., Clausen, H. B., Dahl-Jensen, D., Fis-
 1243 cher, H., ... White, J. W. (2008, 8). High-resolution greenland ice core data
 1244 show abrupt climate change happens in few years. *Science*, *321*, 680-684. doi:
 1245 10.1126/science.1157707
- 1246 Steig, E. J., Ding, Q., White, J. W., Küttel, M., Rupper, S. B., Neumann, T. A., ...
 1247 Korotkikh, E. (2013, 5). Recent climate and ice-sheet changes in west antarctica
 1248 compared with the past 2,000 years. *Nature Geoscience*, *6*, 372-375. doi:
 1249 10.1038/ngeo1778
- 1250 Stevens, C. M., Verjans, V., Lundin, J. M., Kahle, E. C., Horlings, A. N., Hor-
 1251 lings, B. I., & Waddington, E. D. (2020, 9). The community firn model
 1252 (cfm) v1.0. *Geoscientific Model Development*, *13*, 4355-4377. doi:
 1253 10.5194/gmd-13-4355-2020
- 1254 Touzeau, A., Landais, A., Morin, S., Arnaud, L., & Picard, G. (2018, 6). Numerical
 1255 experiments on vapor diffusion in polar snow and firn and its impact on
 1256 isotopes using the multi-layer energy balance model crocus in surfex v8.0. *Geo-*
 1257 *scientific Model Development*, *11*, 2393-2418. doi: 10.5194/gmd-11-2393-2018
- 1258 Town, M. S., , & Steen-Larsen, H. C. (2023). *Water isotopologues of near-surface*
 1259 *polar snow from short (1-m) snow cores, extracted from the eastgrip site on*

- 1260 *greenland ice sheet during summers 2017-2019*. [data set]. PANGAEA. Re-
1261 trieved from PANGAEAdata submission:PDI-33691
- 1262 Town, M. S., Waddington, E. D., Walden, V. P., & Warren, S. G. (2008). Temper-
1263 atures, heating rates and vapour pressures in near-surface snow at the south
1264 pole. *Journal of Glaciology*, *54*.
- 1265 Town, M. S., Warren, S. G., Walden, V. P., & Waddington, E. D. (2008, 12). Effect
1266 of atmospheric water vapor on modification of stable isotopes in near-surface
1267 snow on ice sheets. *Journal of Geophysical Research Atmospheres*, *113*. doi:
1268 10.1029/2008JD009852
- 1269 Uemura, R., Masson-Delmotte, V., Jouzel, J., Landais, A., Motoyama, H., & Stenni,
1270 B. (2012). Ranges of moisture-source temperature estimated from antarctic ice
1271 cores stable isotope records over glacial-interglacial cycles. *Climate of the Past*,
1272 *8*, 1109-1125. doi: 10.5194/cp-8-1109-2012
- 1273 Van Geldern, R., & Barth, J. A. (2012). Optimization of instrument setup and post-
1274 run corrections for oxygen and hydrogen stable isotope measurements of water
1275 by isotope ratio infrared spectroscopy (iris). *Limnology and Oceanography:*
1276 *Methods*, *10*, 1024-1036. doi: 10.4319/lom.2012.10.1024
- 1277 Vinther, B. M., Jones, P. D., Briffa, K. R., Clausen, H. B., Andersen, K. K., Dahl-
1278 Jensen, D., & Johnsen, S. J. (2010, 2). Climatic signals in multiple highly
1279 resolved stable isotope records from greenland. *Quaternary Science Reviews*,
1280 *29*, 522-538. doi: 10.1016/j.quascirev.2009.11.002
- 1281 Waddington, E. D., Steig, E. J., & Neumann, T. A. (2002). Using characteristic
1282 times to assess whether stable isotopes in polar snow can be reversibly de-
1283 posited. *Annals of Glaciology*, *35*, 118-124. doi: 10.3189/172756402781817004
- 1284 Wahl, S., Steen-Larsen, H. C., Reuder, J., & Hörhold, M. (2021, 7). Quantifying
1285 the stable water isotopologue exchange between the snow surface and lower
1286 atmosphere by direct flux measurements. *Journal of Geophysical Research:*
1287 *Atmospheres*, *126*. doi: 10.1029/2020JD034400
- 1288 Wahl, S., Steen-Larsen, H. C., Hughes, A. G., Dietrich, L. J., Zuhr, A., Behrens,
1289 M., ... Hörhold, M. (2022, 10). Atmosphere-snow exchange explains
1290 surface snow isotope variability. *Geophysical Research Letters*, *49*. doi:
1291 10.1029/2022gl099529
- 1292 Werner, M., Jouzel, J., Masson-Delmotte, V., & Lohmann, G. (2018, 12). Rec-

- 1293 oncing glacial antarctic water stable isotopes with ice sheet topography
1294 and the isotopic paleothermometer. *Nature Communications*, *9*. doi:
1295 10.1038/s41467-018-05430-y
- 1296 Werner, M., Langebroek, P. M., Carlsen, T., Herold, M., & Lohmann, G. (2011).
1297 Stable water isotopes in the ecam5 general circulation model: Toward high-
1298 resolution isotope modeling on a global scale. *Journal of Geophysical Research*
1299 *Atmospheres*, *116*. doi: 10.1029/2011JD015681
- 1300 Westhoff, J., Sinnl, G., Svensson, A., Freitag, J., Kjær, H. A., Vallelonga, P.,
1301 ... Weikusat, I. (2022, 5). Melt in the greenland eastgrip ice core re-
1302 veals holocene warm events. *Climate of the Past*, *18*, 1011-1034. doi:
1303 10.5194/cp-18-1011-2022
- 1304 Zuhr, A. M., Münch, T., Steen-Larsen, H. C., Hörhold, M., & Laepple, T. (2021,
1305 10). Local-scale deposition of surface snow on the greenland ice sheet.
1306 *Cryosphere*, *15*, 4873-4900. doi: 10.5194/tc-15-4873-2021
- 1307 Zuhr, A. M., Wahl, S., Steen-Larsen, H. C., Hörhold, M., Meyer, H., & Laepple, T.
1308 (2023). A snapshot on the buildup of the stable water isotopic signal in the
1309 upper snowpack at eastgrip on the greenland ice sheet.

Table 1: All data used in this study listed with units, a brief description, and data source. Uncertainties are 2σ standard deviation around the means.

Data	Units/Res.	Description	reference
Temperature	$-28.5 \pm 14^\circ C$	PROMICE weather station, hourly frequency, 2017-2019	Fausto et al. (2021)
Wind speed	5.26 ± 4.6 m/s	data source and frequency same as above	same as above
Wind direction	W-SW	prevailing wind direction in all seasons, data source and frequency same as above	same as above
Annual accumulation (a)	134-157 mm/year	derived from from snow pits, 2009-2017	Komuro et al. (2021)
Annual accumulation (b)	145, 149 mm/year	snow pits, 2009-2016	Nakazawa et al. (2021)
Surface snow, 2016-2019	$\delta^{18}O = \pm 0.22^\circ/_{\text{‰}}$; $\delta D = \pm 1.6^\circ/_{\text{‰}}$	Daily samples of 0-1 cm snow	Wahl et al. (2022), Section 2.2
Snow profiles, 2017	$\delta^{18}O = \pm 0.22^\circ/_{\text{‰}}$; $\delta D = \pm 1.6^\circ/_{\text{‰}}$; 1-cm res, 0-10 cm; 2-cm res, 10-100 cm	Four (4) transects, 2 May 2017 - 11 August 2017, 40 profiles	Section 2.3
Snow profiles, 2018	same as above	Five (5) transects at six loca- tions, 12 May 2018 - 06 August 2018, 35 profiles	Section 2.3
Snow profiles, 2019	same as above	Five (5) transects, 29 May 2019 - 24 July 2019, 25 profiles	Section 2.3

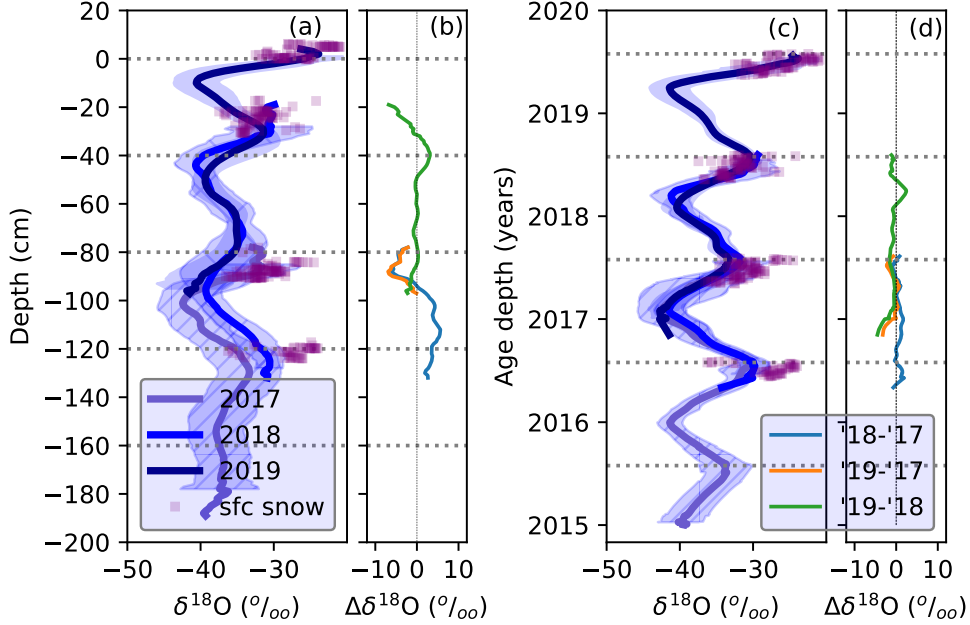


Figure 3: Mean $\delta^{18}O$ values from snow profiles and surface snow. The surface snow data (purple squares) are daily means from the 2016-2019 summer seasons. The snow profiles are mean values grouped by year of extraction (e.g. 2017, 2018, and 2019). Panel (a) shows the mean surface snow and snow profile $\delta^{18}O$ values as a function of relative depth. The surface is defined as 29 May 2019, the first day of snow profile sampling in 2019. Panel (b) shows the difference between each profile as a function of relative depth, representing the interannual change in $\delta^{18}O$. Panel (c) shows the mean surface snow and snow profile $\delta^{18}O$ values as a function of age-depth. Panel (d) shows the difference between each profile as a function of age-depth, representing the interannual change in $\delta^{18}O$. Shading represents 2σ standard error ($2\sigma_{\bar{x}}$). The horizontal lines in panels (a) and (b) are set at 40 cm, the approximate annual accumulation rate at EastGRIP. The horizontal lines in panels (c) and (d) represent 31 July of each year.

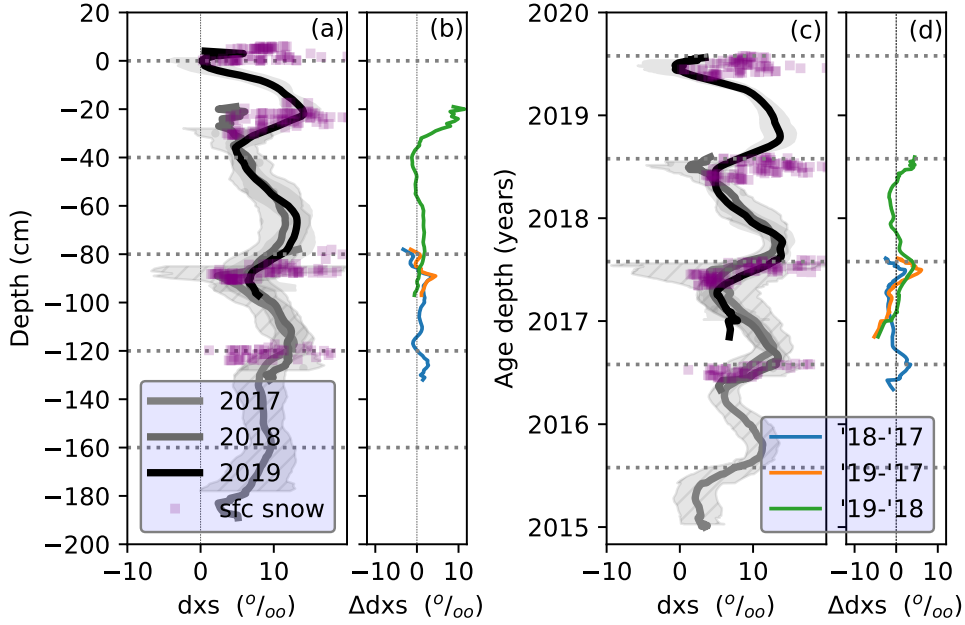


Figure 4: Mean d values from snow profiles and surface snow, as in Figure 3 for $\delta^{18}O$. The surface snow data (purple squares) are daily means from the 2016-2019 summer seasons. The snow profiles are mean values grouped by year of extraction (e.g. 2017, 2018, and 2019) with $2\sigma_{\bar{x}}$ as the shading. Panel (a) shows the mean surface snow and snow profile d values as a function of relative depth. The surface is defined as 29 May 2019, the first day of snow profile sampling in 2019. Panel (b) shows the difference between each profile as a function of relative depth. Panel (c) shows the mean surface snow and snow profile d values as a function of age-depth. Panel (c) shows the difference between each profile as a function of age-depth. Panels (b) and (d) represent the change in d between the different field seasons. Shading represents 2σ standard error ($2\sigma_{\bar{x}}$). The horizontal lines in panels (a) and (b) are set at 40 cm, the approximate annual accumulation rate at EastGRIP. The horizontal lines in panels (c) and (d) represent 31 July of each year.

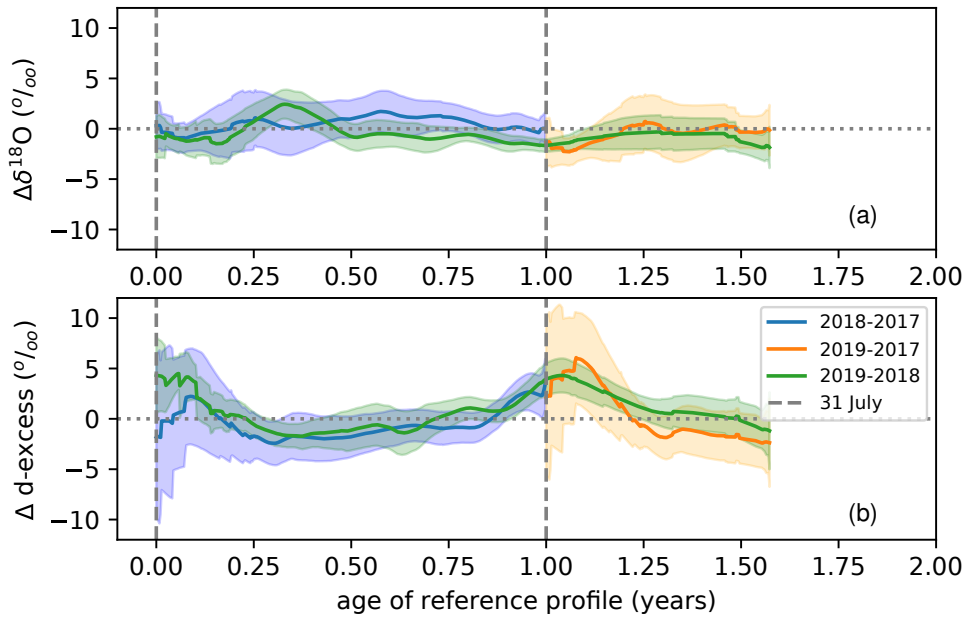


Figure 5: The change in $\delta^{18}\text{O}$ (panel (a)) and d (panel (b)) after one-to-two years of aging in the near surface snow. The change is determined as the difference between profiles shown in Figures 3(c) and 4(c), and plotted as a function of the age of the reference profile in the difference (e.g. 2018-2017 is plotted against the age of each snow layer from 2017). Seasons are marked on the horizontal axis, with snow depth increasing and time decreasing to the right.

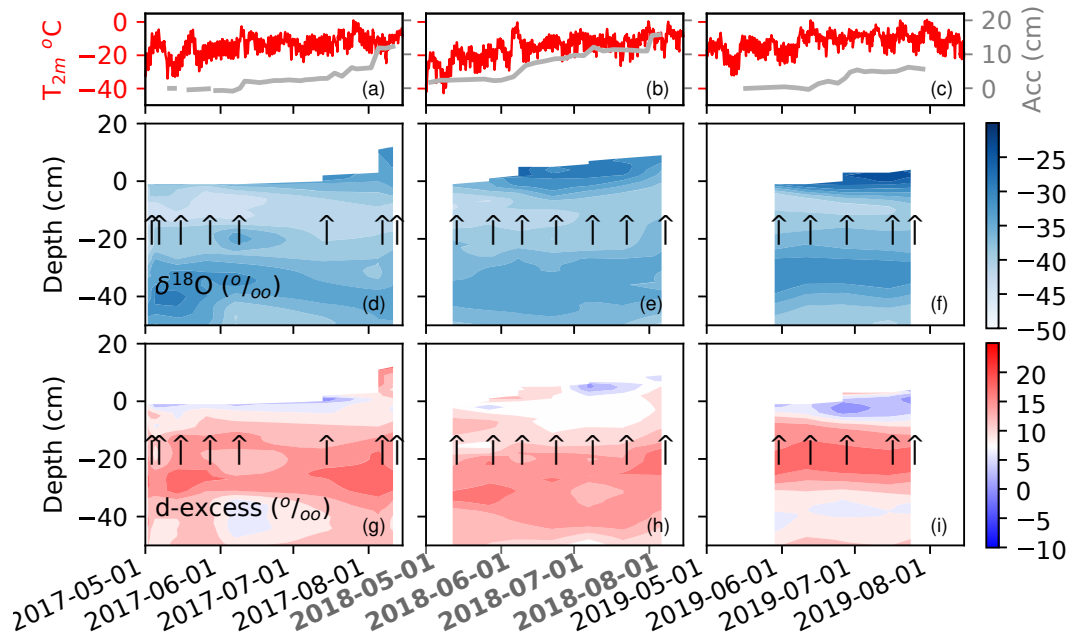


Figure 6: Mean $\delta^{18}\text{O}$ and d snow profiles plotted as depth (vertical axis) and date of extraction (horizontal axis) for the three summer field seasons 2017, 2018, and 2019. Panels (a-c) show the 2-m air temperature from the local PROMICE weather station and accumulation from the bamboo stake field. Panels (d-f) show the $\delta^{18}\text{O}$ content of the near-surface snow determined from mean $\delta^{18}\text{O}$ snow profiles. Each up arrow represents dates snow profiles were taken and averaged. For 2017, each arrow represents a mean of four snow profiles spaced approximately 50 m apart. For 2018 and 2019, each up arrow represents the mean of five snow profiles spaced approximately 50 m apart. Panels (g-i) are similar contour plots but for d . Note the vertical axis only extends to 50 cm depth because there is not subseasonal change below approximately 20-30 cm.

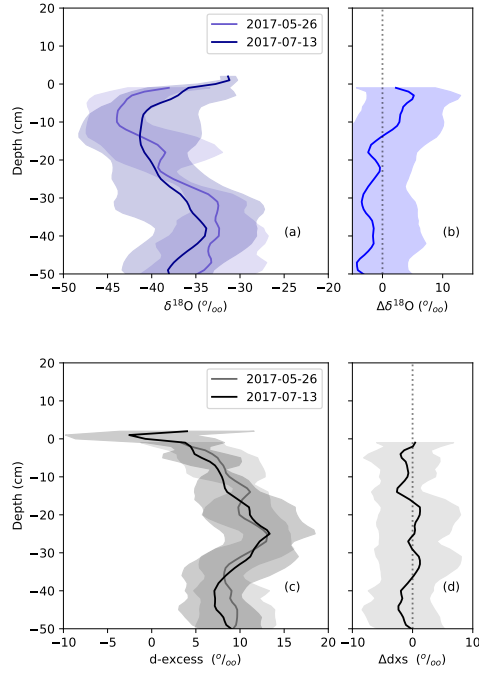


Figure 7: The mean isotopic change in near-surface from a low accumulation period during summer (25 May 2017 and 13 July 2017). Panels (a) and (c) are the mean snow profiles of $\delta^{18}O$ and d computed from four snow profiles each. Panels (b) and (d) show the isotopic change over this time period. Error bars are 2σ standard error.

Table A1: Table of annual statistics for $\delta^{18}O$ from the EastGRIP snow profiles shown in Figure 3. Columns are the year of extraction, e.g. 2019 represents July-July annual average from snow extracted during the 2019 summer field season (also the dark blue curve in Figure 3(c)). Rows are the age of the snow. The annual cycle is winter-centric, and computed from 31 July to 31 July. Units are in ‰ and uncertainty is $2\sigma_{\bar{x}}$.

<i>Extraction year</i>	<i>2017</i>	<i>2018</i>	<i>2019</i>
Annual layer age			
07/2015 - 07/2016	-36.5 ± 1.0	—	—
07/2016 - 07/2017	-37.2 ± 1.1	-36.7 ± 1.0	—
07/2017 - 07/2018	—	-35.7 ± 1.0	-36.0 ± 0.8
07/2018 - 07/2019	—	—	-34.9 ± 1.4

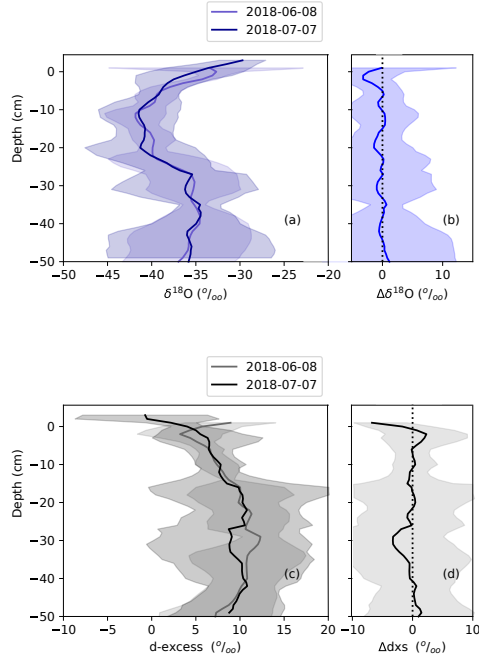


Figure 8: The mean isotopic change in near-surface from a low accumulation period during summer (08 June 2018 and 07 July 2018), similar to Figure 7. Panels (a) and (c) are the mean snow profiles of $\delta^{18}O$ and d computed from five snow profiles each. Panels (b) and (d) show the isotopic change over this time period. Error bars are 2σ standard error.

Table A2: Table of changes in $\delta^{18}O$ concentration after one or two years of aging in the EastGRIP firn from Figures 3(d) and 3(c), respectively. Columns are mean annual residuals, summer residuals (June/July), and non-summer residuals. Rows are the years between which the change is calculated. Units are in ‰ and uncertainty is $2\sigma_{\bar{x}}$.

	<i>Annual</i>	<i>Summer</i>	<i>Non-summer</i>
$\overline{\delta^{18}O}_{y2} - \overline{\delta^{18}O}_{y1}$			
$\overline{\delta^{18}O}_{2018} - \overline{\delta^{18}O}_{2017}$	0.6 ± 0.5	0.3 ± 0.3	0.6 ± 0.5
$\overline{\delta^{18}O}_{2019} - \overline{\delta^{18}O}_{2017}$	-0.9 ± 0.6	-1.6 ± 0.3	-0.7 ± 0.5
$\overline{\delta^{18}O}_{2019} - \overline{\delta^{18}O}_{2018}$	-0.83 ± 0.8	-1.1 ± 0.4	-0.8 ± 0.4

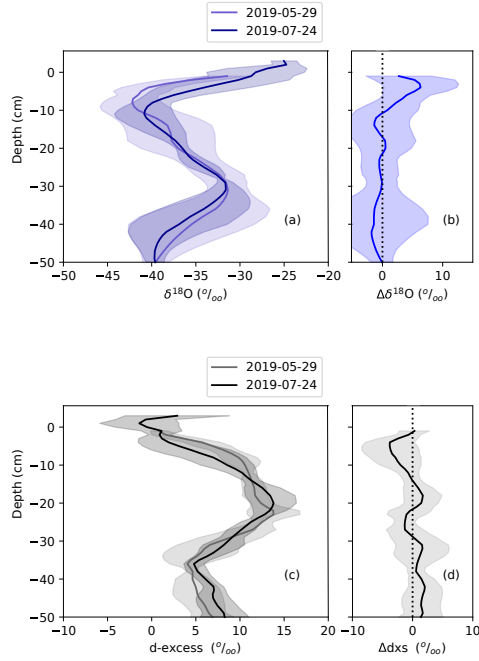


Figure 9: The mean isotopic change in near-surface from a low accumulation period during summer (29 May 2019 and 24 July 2019), similar to Figure 7. Panels (a) and (c) are the mean snow profiles of $\delta^{18}O$ and d computed from five snow profiles each. Panels (b) and (d) show the isotopic change over this time period. Error bars are 2σ standard error.

Table A3: Table of annual statistics for d from the EastGRIP snow profiles shown in Figure 3. Columns are the year of extraction, e.g. *2019* represents the black curve in Figure 4. Rows are the age of the snow. The annual cycle is winter-centric, and computed from 31 July to 31 July. Units are in ‰ and uncertainty is $2\sigma_{\bar{x}}$.

<i>Extraction year</i>	<i>2017</i>	<i>2018</i>	<i>2019</i>
Annual layer age			
07/2015 - 07/2016	8.8 ± 1.0	—	—
07/2016 - 07/2017	8.9 ± 1.1	8.4 ± 0.9	—
07/2017 - 07/2018	—	8.5 ± 1.0	8.9 ± 0.8
07/2018 - 07/2019	—	—	9.0 ± 1.4

Table A4: Table of changes in d concentration after one or two years of aging the East-GRIP firn from Figures 4(a) and 4(c), respectively. Columns are mean annual residuals, summer residuals (June/July), and non-summer residuals. Rows are the years between which the change is calculated. Units are in ‰ and uncertainty is $2\sigma_{\bar{x}}$.

	<i>Annual</i>	<i>Summer</i>	<i>Non-summer</i>
$\bar{d}_{y2} - \bar{d}_{y1}$			
$\bar{d}_{2018} - \bar{d}_{2017}$	-0.37 ± 0.4	1.11 ± 0.6	-0.89 ± 0.4
$\bar{d}_{2019} - \bar{d}_{2017}$	-0.5 ± 0.4	4.3 ± 0.6	-1.8 ± 0.4
$\bar{d}_{2019} - \bar{d}_{2018}$	0.4 ± 0.4	3.3 ± 0.6	-0.3 ± 0.4

Table A5: Table of statistics for $\delta^{18}O$ and d from the EastGRIP surface snow, and d from near-surface summer snow less than one year old, as shown in Figure 3 and 4. Columns are the isotopologues. Rows are the sampling time period. Units are in ‰ and uncertainty is $2\sigma_{\bar{x}}$.

	$\delta^{18}O_{sfc}$, summer	d_{sfc} , summer	d , summer snow profile, < 1 year old
Field season			
06-08/2016	-27.7 ± 1.2	8.55 ± 1.5	
06-08/2017	-31.28 ± 1.4	8.22 ± 2.9	7.76 ± 0.9
06-08/2018	-32.19 ± 1.4	10.31 ± 2.5	5.41 ± 0.54
06-08/2019	-26.39 ± 1.4	8.08 ± 2.4	3.72 ± 0.59

Table A6: Table of $\delta^{18}O$ vs δD composited by age and season. Summer is June-July. Winter is December-April. Units are in $(\text{‰})/(\text{‰})$ and uncertainty is 2σ .

	slope
All data	8.05 ± 0.003
age < 1 year	7.91 ± 0.004
<i>Summer</i>	7.87 ± 0.02
<i>Winter</i>	8.10 ± 0.01
1 year \leq age < 2 years	8.18 ± 0.006
<i>Summer</i>	8.56 ± 0.03
<i>Winter</i>	7.96 ± 0.02

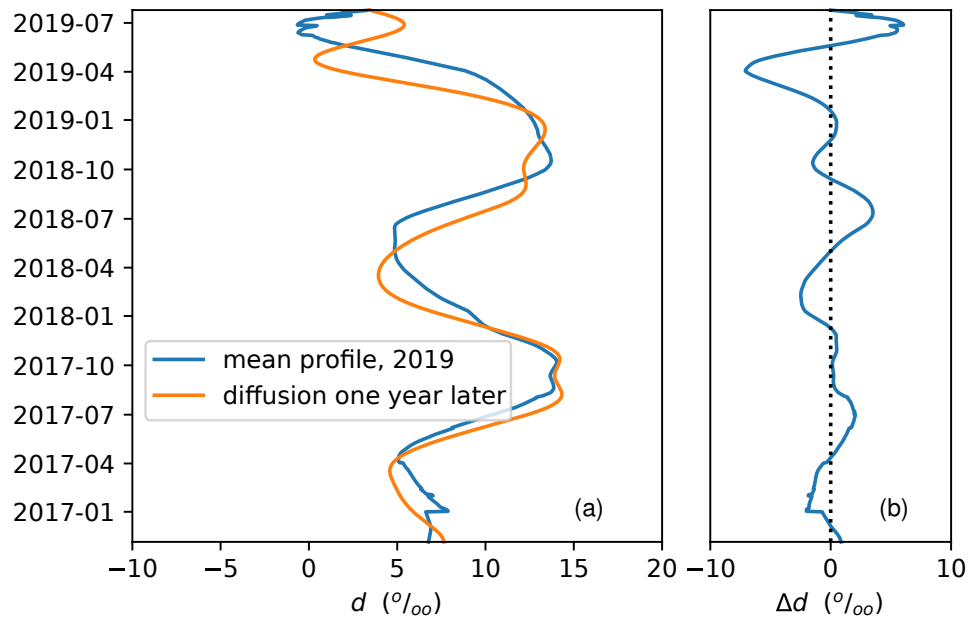


Figure B1: Panel (a) shows a simulation of the impact of isotopic-gradient-driven diffusion on the mean d snow profile from 2019 (blue curve) after one year of aging (orange curve). Panel (b) shows the change in d (Δd) after one year of aging. The simulation is described in detail in this Appendix B1.